Membrane contact sites regulate vacuolar fission via sphingolipid metabolism

Kazuki Hanaoka[1,†], Kensuke Nishikawa[1,†], Atsuko Ikeda[1,†], Philipp Schlarmann[1], Saku Sasaki[1], Sayumi Yamashita[2], Aya Nakaji[2], Sotaro Fujii[1] and Kouichi Funato[1,2*]

[1]Graduate School of Integrated Sciences for Life, Hiroshima University, Kagamiyama 1-4-4, Higashi-Hiroshima 739-8528, Japan.

[2]School of Applied Biological Science, Hiroshima University, Kagamiyama 1-4-4, Higashi-Hiroshima 739-8528, Japan.

[†]These authors contributed equally to this work

* Corresponding author; Kouichi Funato

Email: kfunato@hiroshima-u.ac.jp

Abstract

Membrane contact sites (MCSs) are junctures that perform important roles including coordinating lipid metabolism. Previous studies have indicated that vacuolar fission/fusion processes are coupled with modifications in the membrane lipid composition. However, it has been still unclear whether MCS-mediated lipid metabolism controls the vacuolar morphology. Here we report that deletion of tricalbins (Tcb1, Tcb2, Tcb3), tethering proteins at endoplasmic reticulum (ER)-plasma membrane (PM) and ER-Golgi contact sites, alters fusion/fission dynamics and causes vacuolar fragmentation in the yeast *Saccharomyces cerevisiae*. In addition, we show that the sphingolipid precursor phytosphingosine accumulates in tricalbin-deleted cells, triggering the vacuolar division. Detachment of the nucleus vacuole junction (NVJ), an important contact site between the vacuole and the perinuclear ER, restored vacuolar morphology in both cells subjected to high exogenous phytosphingosine and Tcb3-deleted cells, supporting that phytosphingosine transport across the NVJ induces vacuole division. Thus, our results suggest that vacuolar morphology is maintained by MCSs through the metabolism of sphingolipids.

Introduction

Cellular organelles are formed by membranes with unique lipid compositions, morphology, and functions. The vacuole of budding yeast is an organelle that shares many similarities with mammalian lysosomes and plant vacuoles. Vacuoles possess degradative and storage capacities, and are essential for maintaining cellular homeostasis, including maintaining pH or ion homeostasis, cellular detoxification, and responses to osmotic shock and nutrient environments. Vacuoles are liable to change their morphology (size, volume, and number) through cycles of fusion and fission, to adapt to the intracellular and extracellular environments or upon vacuole inheritance to daughter cells. The steady-state morphology of the vacuole is maintained by a balance of constitutive vacuolar fusion and fission processes [1] [2].

The homotypic vacuolar membrane fusion process occurs in four stages: priming, tethering, docking and fusion [3] [4] [5] [6]. Each stage is defined as follows. “Priming” In the priming reaction, inactive fusion factors that are still assembled from previous fusion events are recycled. The yeast N-ethylmaleimide-sensitive factor (NSF), Sec18p, is activated by ATP and releases the NSF attachment protein (SNAP), Sec17p, from the SNAP receptor (SNARE) complex, thereby activating the SNARE molecule [3] [4] [7]. “Tethering” The HOPS/Class C Vps complex and the Rab-GTPase Ypt7p mediate the reversible contact of opposing vacuoles [4] [8]. “Docking” The coupling of three Q-SNAREs (Vam3p, Vam7p, and Vti1p) with an opposing R-SNARE (Nyv1p) to form a trans-SNARE complex between the two corresponding vacuoles. “Fusion” The final stage in which the lipid bilayer fuses and the contents of the lumen are mixed [5] [7]. For stable vacuolar fusion, several factors are required such as vacuolar acidification by V-ATPase proton pump activity [1] [9] [10] [11], ions [12] and ion transporters [13].

Furthermore, vacuolar fission is required for proper vacuolar inheritance during mitosis and acute response to osmotic shock in yeast, however the molecular mechanism of fission is not fully understood, and limited knowledge is available. Vacuolar fission is performed in two steps that require proteins and lipids [14]. The first step is the contraction and invagination of the vacuolar membrane through the involvement of Vps1p, a dynamin-like GTPase [15] and V-ATPase, which drives the proton gradient [1]. Next, vacuolar fission is promoted by Vac14p, Vac7p, and Fab1p [16], which are required for the generation of PtdIns[3,5]P2, and Atg18p, an effector of Fab1p and a sensor of PtdIns[3,5]P2 levels [17] [18]. Recently, it has also been shown that vacuolar fission is associated with nutrient status and responds to ER stress via TORC1 targets [19] [20]. Moreover, it has been proposed that vacuolar fusion and fission dynamics are regulated by the Yck3p-Env7p kinase cascade, which maintains an equilibrium between fusion and fission activities [21].

Organelles construct a dynamic network by associating with each other through membrane-contact sites (MCSs), which play an important role in lipid transport and metabolism [22] [23]. Lipids (phosphatidic acid (PA), diacylglycerol, ergosterol, phosphatidylinositol (PtdIns) phosphate (PtdInsP)) and lipid raft domains have been shown to be important as fusion and fission effectors and discussed in a variety of recent reviews [2] [17] [24] [25] [26] [27]. However, it remains unclear if MCS-mediated lipid metabolism controls the morphology of the vacuole. Vacuoles have contact sites with other organelles. The MCS where the nuclear ER meets the vacuole is called the nucleus-vacuole junction (NVJ), and the ER-localized Nvj1p and vacuole-membrane-localized Vac8p act as tethers to form the NVJ [28]. Vacuoles also form MCS with mitochondria called vacuole and mitochondria patches (vCLAMP). vCLAMP is mediated by the soluble (cytosol-localized) HOPS complex subunit Vps39p, the vacuole-localized small Rab-GTPase Ypt7p, and by an unknown mitochondrial factor [29] [30]. The translocase of the mitochondrial outer membrane (TOM) subunit Tom40p has been identified as a direct binding partner of Vps39p, suggesting a mechanism for the formation of vCLAMP by the Ypt7p-Vps39p-Tom40p tether [31]. Although it has been suggested that MCSs with vacuoles are involved in the transport of lipids such as sterols and precursors of sphingolipids that are involved in vacuolar morphology [32] [33] [34] [35], the roles of those MCSs-mediated lipid metabolisms in the regulation of vacuole morphology are not understood.

In this study, we found that tether proteins of MCS formation are involved in the regulation of vacuolar morphology. We show that the deletion of tricalbins, tethers of the MCS between the ER and the plasma membrane (PM) [36] and between the ER and the Golgi apparatus [37], affects vacuolar division. Phytosphingosine, a precursor of ceramide, accumulated in the tricalbin-deleted strain and was revealed as the underlying cause that triggers vacuolar fission. Moreover, deletion of key tethering proteins at the NVJ recovered vacuolar morphology of cells subjected to high exogenous phytosphingosine and tricalbin-deleted cells, indicating that the NVJ is required for phytosphingosine-induced vacuolar fission. In summary, we propose that vacuolar morphology is regulated by MCSs through regulation of sphingolipid metabolic pathways.

Results

Deletion of tricalbins causes vacuole fragmentation

Tricalbins (Tcb1p, Tcb2p, and Tcb3p) are ER membrane tethering proteins that connect the cortical ER (cER) with the PM [38], and contribute to PI4P turnover [36], sterol flux and transport [39] and maintain other lipid homeostasis [40]. It is also suggested that tricalbins create ER membrane curvature to maintain PM integrity [41] [42]. Tricalbins also localize to the ER-Golgi contacts and are responsible for the non-vesicular transport of ceramide from ER to Golgi apparatus [37]. However, their role in other organelle morphology and function remains unknown. Interestingly, the *NVJ1* gene, which encodes a major component of the NVJ, showed a negative synthetic interaction with the absence of all three tricalbins (*tcb1*Δ*2*Δ*3*Δ) [41]. Moreover, HOPS subunit Vam6p and Rab-GTPase Ypt7p, which are both involved in vacuolar fusion, also showed negative synthetic interaction with *tcb1*Δ*2*Δ*3*Δ [41]. Based on the findings, we assumed that tricalbins may be involved in the regulation of vacuolar morphology or function linked with the NVJ. To investigate the role of tricalbins in vacuole morphology, we analyzed the number of vacuoles per cell by a fluorescent probe FM4-64 that selectively stains yeast vacuolar membranes. We observed that compared to wild type cells, the *tcb1*Δ*2*Δ*3*Δ strain showed a phenotype characterized by a decreased percentage of cells with one vacuole and an increased percentage of cells with two or more vacuoles (Fig 1A). We refer to this phenotype as vacuolar fragmentation. In addition, analysis with single- and double deletion strains revealed that single deletion of *TCB1* or *TCB3* already exhibited strong vacuole fragmentation (Fig 1B). These results indicate that tricalbins are important to maintain vacuole morphology.

We next examined whether deletion of tricalbins affects vacuolar acidification. As homotypic vacuole-vacuole membrane fusion requires the vacuolar H^+-ATPase (V-ATPase) [11] [43] [44], tricalbins could be indirectly involved in maintaining vacuole morphology through V-ATPase. Therefore, we addressed whether tricalbin mutant strains could grow in alkaline media, because V-ATPase–deficient mutants can grow in acidic media but fail to grow in alkaline media [43]. As a negative control, we used *vma3*Δ mutant cells in which one of the V_O subunits of V-ATPase had been deleted. The *vma3*Δ mutant cells grew in acidic medium (pH 5.0), but failed to grow in alkaline medium (pH 7.5) (Fig S1A). In contrast, all tricalbin mutant strains grew like wild type in both conditions, suggesting that the V-ATPase in these mutants remains functionally normal. Thus, these results suggest that vacuole fragmentation caused by tricalbin deletion is not due to a loss of function of V-ATPase.

Furthermore, we investigated the effects of tricalbin deletion on delivery of a vacuolar protease, carboxypeptidase S (Cps1p) that is sorted into the vacuole lumen upon endosome–vacuole fusion. Deletion of HOPS complex components that mediate endosome–vacuole fusion

results in vacuole fragmentation [45]. To test the possibility that vacuole fragmentation in tricalbin mutant cells is caused by a defect of endosome–vacuole fusion, we analyzed the localization of GFP-Cps1p in tricalbin mutant cells. Cps1p, a vacuole-localized hydrolytic enzyme, is transported to the vacuole after sorting into multivesicular bodies by ESCRT (endosomal sorting complex required for transport) recognition [46]. In strains with loss of ESCRT function, such as disruption of *VPS4*, one of the class E *VPS* (vacuolar protein sorting) genes, GFP-Cps1p is known to localize to the limiting membrane rather than the lumen of the vacuole [47] [48]. In both WT and *tcb3*Δ cells, GFP-Cps1p was observed in the vacuole lumen in contrast to *vps4*Δ cells (Fig S1B), suggesting that the tricalbin mutant exhibits a normal delivery of vacuolar proteins via endosomes to the vacuole. In addition, the fact that tricalbin deletion does not affect the maturation of CPY, a vacuolar hydrolase carboxypeptidase Y [37], indicates that the vacuolar degradation ability as well as protein delivery to the vacuole is normal. Taken together, tricalbins are required for maintaining vacuole morphology, but not due to an indirect action through vacuolar acidification or endosome-vacuole fusion.

Tricalbins negatively regulate vacuole fission in a parallel pathway with TORC1

The number and size of vacuoles within a cell are regulated by coordinated cycles of vacuolar fission and fusion. To address whether vacuole fragmentation in the tricalbin mutant is caused by facilitation of vacuole fission or an impaired homotypic vacuole fusion, we examined the effect of hypotonic stress on vacuole fragmentation in *tcb1*Δ*2*Δ*3*Δ mutant cells, because low-osmotic stimuli such as water promote homotypic vacuole fusion to maintain cytoplasmic osmolarity [49]. We observed that addition of water to *tcb1*Δ*2*Δ*3*Δ cells partially restored vacuole fragmentation, suggesting that vacuolar fusion machinery is functional in *tcb1*Δ*2*Δ*3*Δ cells (Fig 1C). This result suggests that loss of tricalbins alters fusion-fission dynamics by primarily affecting the fission machinery rather than fusion.

As the target of rapamycin complex 1 (TORC1) is a positive regulator of vacuole fission in response to hyperosmotic shock and ER stress [19] [20], we next examined if rapamycin, which is an inhibitor of TORC1, affects the vacuole fragmentation in *tcb1*Δ*2*Δ*3*Δ cells. As shown in Figure 1C, we observed that the vacuole fragmentation in *tcb1*Δ*2*Δ*3*Δ cells was suppressed by rapamycin, suggesting that TORC1 may be required for tricalbin deletion-induced vacuolar fragmentation. We attempted to characterize further the relationship between tricalbin and TORC1, and showed that *tcb1*Δ*2*Δ*3*Δ cells had no significant effect on phosphorylation levels of Sch9p, a major downstream effector of TORC1 (Fig 1D). These results suggest that deletion of tricalbins does not activate TORC1. Therefore, we conclude that tricalbins and TORC1 act in parallel and opposite ways to regulate vacuole fission (Fig 1E).

The transmembrane domain of Tcb3 contributes to mediating protein interactions between the tricalbin family to maintain vacuolar morphology

Tcb3p possesses an N-terminal transmembrane (TM) domain, a central synaptotagmin-like mitochondrial lipid-binding protein (SMP) domain, and multiple C-terminal Ca^{2+}-dependent lipid binding (C2) domains (Fig 2A). To identify which domain of Tcb3p is essential for regulating vacuole fission, we replaced the C-terminal sequence of the endogenous *TCB3* gene with a GFP binding protein (GBP). This way, we created three strains expressing either full-length Tcb3-GBP; Tcb3(Full)-GBP, Tcb3-GBP lacking C2 domains; Tcb3(TM-SMP)-GBP or Tcb3-GBP lacking both SMP and C2 domains; Tcb3(TM)-GBP. Vacuole morphology in cells expressing Tcb3(Full)-GBP (Fig 2B (iii)) was almost similar to that in WT cells (Fig 2B (i)), indicating that the addition of GBP has no effect on vacuole morphology. Remarkably, vacuoles remained non-fragmented even in cells expressing Tcb3(TM)-GBP, which lacked most of the C-terminal region (Fig 2B (v)), as well as Tcb3(TM-SMP)-GBP (Fig 2B (iv)). In an attempt to address the question of why the TM domain of Tcb3p is sufficient to suppress vacuolar division, we found that cells expressing Tcb3(TM)-GBP and lacking Tcb1p and Tcb2p (Fig 2B (vi)) are even more fragmented than *tcb1*Δ*2*Δ in Fig 1B, and similar to *tcb3*Δ (Fig 1B and Fig 2B (ii)). These results suggest that the TM domain of Tcb3p requires Tcb1p and Tcb2p to suppress vacuole fission. Tcb2p has been reported to interact with either Tcb1p or Tcb3p through their C-terminal domain [50], and some of the protein interactome analyses have reported that Tcb1p, Tcb2p and Tcb3p interact with each other [51] [52]. In this study, we have also confirmed that Tcb3 shows physical interaction with both Tcb1 and Tcb2 by the coimmunoprecipitation assay (Fig S2). In addition, according to the structural simulation by AlphaFold2, each TM domain of Tcb1p, Tcb2p, and Tcb3p formed alpha-helical structure, which is known to be typical for membrane proteins (Fig 2C). It is likely that Tcb1p and Tcb2p directly interact with Tcb3p by their TM domains. Interestingly, the complex of these three TM domains was constructed with Tcb3p between Tcb1p and Tcb2p in most cases (Fig 2D). Together these data suggest that the TM domain of Tcb3p contributes sufficiently to the maintenance of vacuolar morphology by mediating the tricalbin complex formation (Fig 2E).

Accumulated phytosphingosine in tricalbin-deleted cells causes vacuole fragmentation.

To understand how the deletion of tricalbins leads to vacuole fragmentation, we examined the involvement of lipids. Previous reports showed that levels of acylceramides, which are made by adding another acyl chain to ceramides, increased in *tcb1*Δ*2*Δ*3*Δ cells [37], and levels of long-chain bases (LCBs) increased in Δtether cells lacking six ER-PM tethering proteins [53]. Here we measured lipids in *tcb1*Δ*2*Δ*3*Δ cells by *in vivo* labeling with [^{3}H] dihydrosphingosine (DHS), which is a precursor of phytosphingosine (PHS), and observed significant increases in ceramide species, phosphatidylethanolamine (PE), PHS, phosphatidylinositol (PI), complex

sphingolipids such as inositolphosphorylceramide (IPC) and mannosyl-inositolphosphorylceramide (MIPC) and LCB-1P (DHS-1P/PHS-1P) levels (Fig 3A).

We first evaluated whether the increases in certain lipids are the cause of vacuolar fragmentation in *tcb1*Δ*2*Δ*3*Δ. Our analysis showed that vacuoles are fragmented in *lag1*Δ*lac1*Δ cells, which lack both enzymes for LCBs (DHS and PHS) conversion into ceramides (Fig 3B). Loss of ceramide synthases could cause an increase in PHS levels. Therefore, we tested if exogenously added PHS induces vacuolar fragmentation in WT cells. As shown in Fig 3C, exogenous addition of PHS induced vacuolar fragmentation. PHS are converted into ceramide by the ceramide synthase Lag1p, which is the main enzyme synthesizing phytoceramide [54]. Thus, we next examined whether PHS-induced vacuolar fragmentation occurs in *lag1*Δ cells. Our analysis showed that vacuolar fragmentation in *lag1*Δ cells treated with PHS was comparable to that for WT cells (Fig 3C). These results suggest that the increases in ceramide and subsequent product IPC/MIPC are not the cause of vacuolar fragmentation, but rather its precursors induce vacuolar fragmentation.

Because our lipid analysis showed a strong increase in LCB-1P in *tcb1*Δ*2*Δ*3*Δ cells, phosphorylation of PHS may be involved in PHS-induced vacuolar fragmentation. Although exogenously added LCBs move slowly from the PM to the ER if they are not phosphorylated, efficient utilization of exogenously added LCBs in sphingolipid synthesis requires a series of phosphorylation and dephosphorylation steps for LCBs [55]. The major yeast LCB phosphate phosphatase Lcb3p dephosphorylates LCB-1P (DHS-1P/PHS-1P) to yield DHS/PHS [56], while Lcb4p and Lcb5p catalyze the reverse reaction producing DHS-1P/PHS-1P [57]. Lcb3p, Lcb4p, and Lcb5p are localized to the ER, PM or Golgi [55] [58] [59] [60]. We examined the ability of exogenous PHS to fragment vacuoles in cells lacking these processing factors. Our results showed that PHS-induced vacuolar fragmentation was completely blocked in the *lcb3*Δ cells in which PHS-1P is not dephosphorylated (Fig 3D), suggesting that PHS-induced vacuolar fragmentation requires the reaction of dephosphorylation of PHS-1P by Lcb3p. On the other hand, we observed that vacuoles were still fragmented in *lcb4*Δ *lcb5*Δ and *lcb3*Δ *lcb4*Δ *lcb5*Δ cells (Fig 3D). These results suggest that elevated levels of non-phosphorylated PHS induces vacuolar fragmentation (Fig 3E). Additionally, we tested whether overexpression of Rsb1p, which has been reported as a translocase that exports LCBs from the inner to the outer leaflet of the PM [61], rescues vacuole fragmentation in *tcb1*Δ*2*Δ*3*Δ cells. As shown in Fig 3F, we observed that Rsb1p overexpression results in decreased vacuole fragmentation. Collectively, these results support the model in which vacuole fragmentation in tricalbin-deleted cells is caused by increased levels of PHS.

The nucleus-vacuole junction (NVJ) is required for PHS- or *tcb3*Δ-induced vacuole fragmentation

To characterize further the relationship between PHS and vacuole morphology, we asked whether PHS delivered from the ER to the vacuole induces vacuole fragmentation. We hypothesized that if PHS are transported to the vacuole by either the vesicular transport pathway through the Golgi apparatus or the non-vesicular transport pathway via inter-organellar MCS triggers vacuole fission, then blockage of the transport could rescue the PHS-induced vacuole fragmentation. Accordingly, we used two types of mutant strains, one blocking vesicular transport and the other blocking the NVJ. In a temperature sensitive *sec18-20* mutant, vesicular transport is abolished at the restrictive temperature of 30 ºC or higher, but even at the permissive temperature of 25 ºC, vesicular transport is partially impaired [62]. As shown in Fig 4A (left), under the condition without exogenous PHS, some vacuoles in *sec18-20* mutant cells became fragmented when shifted to the non-permissive temperature of 30 ºC. We also observed that vacuoles in *sec18-20* mutant at 30 ºC underwent fragmentation after addition of PHS to the same extent as at the permissive temperature of 25 ºC (Fig 4A, right), suggesting that vesicle-mediated transport is not required for PHS-induced vacuolar fragmentation. To test the role of NVJ-mediated membrane contact for PHS-induced vacuolar fragmentation we employed a quadruple Δ*NVJ* mutant (*nvj1*Δ *nvj2*Δ *nvj3*Δ *mdm1*Δ) that was used in a previous study in which complete loss of the NVJ was observed [63], but thus has a different background to other strains of this study. When PHS was added to the Δ*NVJ* mutant, we observed a significant suppression of vacuole fragmentation compared to WT (Fig 4B). Finally, to investigate the requirement for NVJ in tricalbin deletion-induced vacuolar fragmentation, we constructed the *tcb3*Δ *nvj1*Δ and *tcb*3Δ *nvj1*Δ *nvj2*Δ *nvj3*Δ *mdm1*Δ mutants. *TCB3* single disruption sufficiently induced vacuolar fragmentation (Fig 1B), whereas as expected, the fragmentation was partially suppressed by loss of only *NVJ1* and completely suppressed by loss of all NVJ factors (*NVJ1*, *NVJ2*, *NVJ3*, and *MDM1*) (Fig 4C). Taken together, we conclude from these findings that vacuole fission caused by accumulated PHS in tricalbin deleted cells requires contact between ER and vacuole at the NVJ, possibly as a way to transport PHS to the vacuole.

NVJ and PHS accumulation mediate hyperosmotic shock-induced vacuole fission

Besides PHS-induced vacuolar fission, it is generally well-known that vacuolar division can be triggered as an acute response to osmotic shock. We made an interesting observation under hyperosmotic conditions (0.2 M NaCl), wherein the loss of NVJ led to complete suppression of vacuolar division (Fig 5A). This finding suggests a significant role for NVJ in vacuolar fission as a hyperosmotic response. To test the involvement of PHS accumulation in this

process, we analyzed the effect of hyperosmolarity on PHS levels. Analysis of PHS under hyperosmotic shock conditions (0.2 M NaCl), in which vacuolar fragments were observed, showed an increase in PHS of about 10% (Fig 5B). Furthermore, when the NaCl concentration was increased to 0.8 M, PHS levels increased up to 30%. While NaCl treatment increased PHS, both ceramide and IPC decreased. There are at least two possible reasons why NaCl increases PHS and decreases ceramide and IPC. The first is the possibility that NaCl dissociates subunits of ceramide synthase (Lag1p, Lac1p, and Lip1p) or IPC synthase (Aur1p and Kei1p). The second possibility is that NaCl suppresses the expression of ceramide synthase or IPC synthase, as can be inferred from the previous report [64]. Alternatively, we cannot exclude the possibility that the difference in PHS levels detected with [^{3}H]DHS in this study is due to differences in the activity of Sur2p hydroxylase that catalysis the conversion of DHS to PHS [65]. Finally, NaCl-induced vacuolar fragmentation, like that caused by PHS treatment, was also suppressed by PHS export from the cell by Rsb1p overexpression (Fig 5C). These results suggest that hyperosmotic shock-induced vacuole fission is also mediated by PHS accumulation and NVJ.

Discussion

In the present study, we found that the accumulation of PHS triggers the fission of vacuoles. Our results suggest that MCSs are involved in this process in two steps. First, the intracellular amount of PHS is modulated by tricalbin-tethered MCSs between the ER and PM or Golgi (Fig 4D left). Second, the accumulated PHS in the tricalbin-deleted cells induces vacuole fission via most likely the NVJ (Fig 4D right). Thus, we propose that MCSs regulate vacuole morphology via sphingolipid metabolism. Fundamental questions that arise from our data concern the accumulation of PHS in the tricalbin deletion strain and the mechanism of PHS-induced vacuole fission. Possible mechanisms for elevated PHS levels in tricalbin-deleted cells are the following. MCS deficiency between ER and PM has been shown to reduce the activity of Sac1p, a PtdIns4P phosphatase [36]. Sac1p disruption strain decreases the levels of complex sphingolipids such as IPC and MIPC, while it increases the levels of their precursors, ceramide, LCB, and LCB-1P [66]. This is probably due to the loss of function of Sac1p, which reduces the level of PtdIns used for IPC synthesis, thereby impairing IPC synthesis, and resulting in the accumulation of precursors such as the substrate ceramide. This model is also consistent with the results of accumulated PtdIns4P and reduced IPC synthesis in Δtether cells [53]. As tricalbins are required for ceramide nonvesicular transport from the ER to the Golgi [37], it is also possible that impaired ceramide nonvesicular transport due to tricalbin deficiency causes ceramide and its precursor, LCB, to accumulate in the ER. Another possibility is that MCS facilitate PHS diffusion

between the ER and the PM, which might be coordinated with the LCB export from the PM by Rsb1p. The loss of tricalbins partially disrupts the ER-PM tether, possibly resulting in low efficiency of PHS ejection by Rsb1p. This is supported by the result that overexpression of Rsb1p suppressed vacuolar fragmentation in tricalbin-deleted cells (Fig 3F).

Previous studies have observed that myriocin treatment results in vacuolar fragmentation [67] [68]. Myriocin treatment itself causes not only the depletion of PHS but of complex sphingolipids such as IPC. This suggests that normal sphingolipid metabolism is important for vacuolar morphology. The reason for this is unclear, but perhaps there is some mechanism by which sphingolipid depletion affects, for example, the recruitment of proteins required for vacuolar membrane fusion. In contrast, our new findings show that PHS increase causes vacuole fragmentation. Taken together, there may be multiple mechanisms controlling vacuole morphology by both increasing and decreasing PHS.

Based on the fact that both PHS- and tricalbin deletion-induced vacuolar fragmentations were partially suppressed by the lack of NVJ (Fig 4B, 4C), it is possible that the trigger for vacuolar fragmentation is NVJ-mediated transport of PHS into the vacuole. Recently, it has been reported that sphingoid bases are transferred between ER and vacuole via the NVJ, and that Mdm1p, a key tethering protein for the formation of the NVJ, may play an additional role in LCB transfer [35]. The study applied an experimental method that tracks LCBs released in the vacuole and showed that Mdm1p is necessary for LCBs leakage into the ER. However, assuming that Mdm1p transports LCBs along its concentration gradient we consider that under normal conditions, LCBs is transported from the ER (as the organelle of PHS synthesis) to the vacuole. Perhaps, Mdm1p may be responsible for pulling out and passing LCBs. However, we cannot rule out the possibility that the repression of vacuolar fragmentation in the absence of NVJ is not due to inhibition of PHS transfer, but rather to changes in the lipid composition of the vacuolar membrane caused by the lack of supply of other substances capable of triggering vacuolar fragmentation other than PHS, like sterols and lipids such as PtdIns[3,5]P2 and its precursors. Further analysis in this regard is warranted.

How accumulated PHS triggers vacuolar fragmentation remains undetermined. Fab1p, a target of TORC1, is responsible for the production of PtdIns[3,5]P2, which is a well-established inducer of vacuolar fragmentation. Fab1p exhibits co-localization with the TORC1-activating EGO complex, and its activity is controlled by Ivy1p [69] and TORC1 [70]. PtdIns[3,5]P2 was shown to regulate vacuole fission employing Vps1p and Atg18p as executioners [71] while also promoting TORC1 activity in a positive feedback loop [72]. In this context, we found that PHS-induced vacuolar fragmentation can be suppressed by the loss of Fab1p and its regulatory binding partner Vac14p (Fig S3). This observation suggests that PHS-induced vacuolar fragmentation would employ known factors such as Fab1p or Vac14p as the executioners.

The following possibilities still remain, although less likely than the above. Sphingosine, as a bioactive lipid, has been reported to exert effects on enzyme activity in humans and yeast [73] [74] [75], and it is possible that PHS may induce vacuolar fragmentation through established signaling pathways. Yabuki et al [75] reported that LCB accumulation activates a signaling pathway that includes major yeast regulatory kinases such as Pkh1/2p, Pkc1p and TORC1, which may be a candidate to promote vacuolar fragmentation. On the other hand, it was shown that membrane division is mediated by certain proteins that contain amphipathic helices (AHs) and interact with lipid cofactors such as PtdIns[4,5]P2, PA, and cardiolipin [76]. Thus, PHS may possess a similar regulatory function as a lipid cofactor for the activity of fission-inducing proteins. If PHS-induced vacuole fragmentation is not due to signaling, another possible model is that PHS accumulation in the vacuolar membrane causes physical changes in the membrane structure that result in membrane fragmentation. The accumulation of sphingosine in the GARP mutant *vps53*Δ, in which retrograde transport from the endosome to the Golgi is blocked, caused vacuolar fragmentation [67], and thus also supports this model. Sphingosine stabilizes (rigidifies) the gel domains in the membrane, leading to a structural defect between the phase separation of "more rigid" and "less rigid" domains [77]. This structural defect may result in high membrane permeability. Sphingosine also forms small and unstable channels (compared to the channels formed by ceramide) in the membrane [78]. Sphingosine channels are not large enough to release proteins but are believed to induce a permeability transition. Other studies have suggested that sphingosine induces non-lamellar structures by interacting with negatively charged lipids such as PA [79]. PHS alone or in concert with negatively charged lipids such as PtdIns[3,5]P2 may be actively involved in the fission process by inducing structural changes in the vacuolar membrane.

Finally, additional results provided further insight into the more general aspects of PHS involvement in the vacuole fission process. Lipid analysis under hyperosmotic shock condition (0.2 M of 0.8 M of NaCl) showed an increase in PHS level (Fig 5B). NaCl-induced vacuolar fragmentation was also suppressed by Rsb1p-mediated PHS export (Fig 5C), as was NVJ loss (Fig 5A). In addition to the hyperosmotic shock-induced PHS accumulation, we have previously shown that treatment with tunicamycin, which is ER stress inducer, increased the PHS level by about 20% [75]. Tunicamycin treatment has been shown to induce vacuole fission [20]. Collectively, we propose that the NVJ and PHS play a general regulatory role in vacuolar morphology.

Materials and Methods

Yeast strains

All strains of *S. cerevisiae* used for this work are listed in Supplementary Table 1.

Plasmids

All plasmids used for this work are listed in Supplementary Table 2.

Culture conditions

Yeast cells were grown either in rich YPD medium (2% glucose, 1% yeast extract, 2% peptone) or in synthetic minimal SD medium (2% glucose, 0.15% yeast nitrogen base, 0.5% ammonium sulfate, bases as nutritional requirements) and supplemented with the appropriate amino acids.

FM4-64 stain and Fluorescence Microscopy

Yeast cells were cultured in YPD medium at 25°C for 15 hours to achieve OD_{600} = 0.5. The cells were collected and suspended in the same medium to achieve OD_{600}=20. 20 mM FM4-64 (N-(3-Triethylammoniumpropyl)-4-(6-(4-(diethylamino) phenyl) hexatrienyl) pyridinium) dissolved in DMSO was added (a final concentration of 20 μM) while shielded from light. The cells were incubated with FM4-64 for 15 minutes at 25°C and then the cells were washed twice with YPD medium. Cells were suspended to achieve OD_{600}=10 in the same YPD medium or YPD containing reagents (such as rapamycin or PHS), and incubated at 25°C for 2 hours under light shielding to label the vacuoles. After incubation, cells were collected and observed with a fluorescence microscope.

Western Blotting

To analyze Sch9 phosphorylation, protein extracts from cells expressing SCH9-5HA were treated with 2-nitro-5-thiocyanobenzoic acid overnight, resolved by SDS-PAGE, immunoblotted, and visualized using rat anti-HA monoclonal antibody (3F10; Roche) and anti-rat IgG antibody (A9037; Sigma-Aldrich) produced in goat. Bands were quantified using ImageJ to determine the relative amounts of phosphorylated Sch9.

Coimmunoprecipitation

Coimmunoprecipitation experiment was performed as described in [80] and [81]. The ER-enriched fraction was solubilized by treatment with 5% digitonin for 1h at 4°C, treated with blocked agarose beads (chromotek) then immunoprecipitated with GFP-Trap agarose beads (chromotek). The immunoprecipitated GFP protein complexes were separated by SDS-PAGE and analyzed by immunoblot.

Lipid Labelling with [^{3}H]DHS

In vivo labelling of lipids with [^{3}H]DHS was carried out as described [82]. Radiolabeled lipids were extracted with chloroform-methanol-water (10:10:3, vol/vol/vol), and analyzed by thin-layer chromatography (TLC) using a solvent system (Chloroform-methanol-4.2N ammonium hydroxide (9:7:2, vol/vol/vol)). Radiolabeled lipids were visualized and quantified on an FLA-7000 system.

Protein complex modelling

The modeled Tcb1p, Tcb2p, and Tcb3p structures were obtained from AlphaFold2 Protein Structure Database (https://alphafold.ebi.ac.uk/). Based on the modeled structures, the amino acids of TM regions were predicted as 79-171 for Tcb1p, 79-162 for Tcb2p, and 189-268 for Tcb3p. The protein complex structures of the TM regions in Tcb1p, Tcb2p, and Tcb3p were modelled by AlphaFold2 program [83] worked on the AlphaFold Colab web space (https://colab.research.google.com/github/deepmind/alphafold/blob/main/notebooks/AlphaFold.ipynb#scrollTo=pc5-mbsX9PZC). The figures were drawn using PyMOL software provided by Schrödinger, Inc. (https://pymol.org/2/).

Data and Materials Availability Statement

The data and materials that support the findings of this study are included in the article and its Supplemental Information, or are available from the corresponding authors on request.

Acknowledgments

We thank Takashi Toda and Masashi Yukawa for GBP-plasmid, Mike Henne for the Δ*NVJ* strain, and Howard Riezman for GFP-*CPS1* plasmid. This research was supported by JSPS KAKENHI 21K20572 and 22K14863 to A.I., 19H02922 and 21K19088 to K.F.

Author Contributions

K.N., A.I. and K.F. designed research; K.H., K. N., A.I., S.Y., A.N. and S.F. performed research; A.I. analyzed data; and A.I., P.S. and K.F. wrote the paper.

Competing Interest Statement

The authors declare no competing interest.

References

1. Baars, T. L., Petri, S., Peters, C., & Mayer, A. (2007). Role of the V-ATPase in regulation of the vacuolar fission-fusion equilibrium. *Molecular biology of the cell*, *18*(10), 3873–3882. doi:10.1091/mbc.e07-03-0205. https://doi.org/10.1091/mbc.e07-03-0205
2. Li, S. C., & Kane, P. M. (2009). The yeast lysosome-like vacuole: endpoint and crossroads. *Biochimica et biophysica acta*, *1793*(4), 650–663. doi:10.1016/j.bbamcr.2008.08.003. https://doi.org/10.1016/j.bbamcr.2008.08.003
3. Wickner, W., & Haas, A. (2000). Yeast homotypic vacuole fusion: a window on organelle trafficking mechanisms. *Annual review of biochemistry*, *69*, 247–275. doi:10.1146/annurev.biochem.69.1.247. https://doi.org/10.1146/annurev.biochem.69.1.247
4. Ostrowicz, C. W., Meiringer, C. T., & Ungermann, C. (2008). Yeast vacuole fusion: a model system for eukaryotic endomembrane dynamics. *Autophagy*, *4*(1), 5–19. doi:10.4161/auto.5054. https://doi.org/10.4161/auto.5054
5. Wickner W. (2010). Membrane fusion: five lipids, four SNAREs, three chaperones, two nucleotides, and a Rab, all dancing in a ring on yeast vacuoles. *Annual review of cell and developmental biology*, *26*, 115–136. doi:10.1146/annurev-cellbio-100109-104131. https://doi.org/10.1146/annurev-cellbio-100109-104131
6. Qiu Q. S. (2012). V-ATPase, ScNhx1p and yeast vacuole fusion. *Journal of genetics and genomics = Yi chuan xue bao*, *39*(4), 167–171. doi:10.1016/j.jgg.2012.02.001. https://doi.org/10.1016/j.jgg.2012.02.001
7. Müller, O., Bayer, M. J., Peters, C., Andersen, J. S., Mann, M., & Mayer, A. (2002). The Vtc proteins in vacuole fusion: coupling NSF activity to V(0) trans-complex formation. *The EMBO journal*, *21*(3), 259–269. doi:10.1093/emboj/21.3.259. https://doi.org/10.1093/emboj/21.3.259
8. Ho, R., & Stroupe, C. (2016). The HOPS/Class C Vps Complex Tethers High-Curvature Membranes via a Direct Protein-Membrane Interaction. *Traffic (Copenhagen, Denmark)*, *17*(10), 1078–1090. doi:10.1111/tra.12421. https://doi.org/10.1111/tra.12421

483 9. Ungermann, C., Wickner, W., & Xu, Z. (1999). Vacuole acidification is required for trans-
484 SNARE pairing, LMA1 release, and homotypic fusion. *Proceedings of the National*
485 *Academy of Sciences of the United States of America*, *96*(20), 11194–11199.
486 doi:10.1073/pnas.96.20.11194. https://doi.org/10.1073/pnas.96.20.11194
487 10. Peters, C., Bayer, M. J., Bühler, S., Andersen, J. S., Mann, M., & Mayer, A. (2001). Trans-
488 complex formation by proteolipid channels in the terminal phase of membrane
489 fusion. *Nature*, *409*(6820), 581–588. doi:10.1038/35054500.
490 https://doi.org/10.1038/35054500
491 11. Desfougères, Y., Vavassori, S., Rompf, M., Gerasimaite, R., & Mayer, A. (2016). Organelle
492 acidification negatively regulates vacuole membrane fusion in vivo. *Scientific reports*, *6*,
493 29045. doi:10.1038/srep29045. https://doi.org/10.1038/srep29045
494 12. Starai, V. J., Thorngren, N., Fratti, R. A., & Wickner, W. (2005). Ion regulation of
495 homotypic vacuole fusion in Saccharomyces cerevisiae. *The Journal of biological*
496 *chemistry*, *280*(17), 16754–16762. doi:10.1074/jbc.M500421200.
497 https://doi.org/10.1074/jbc.M500421200
498 13. Qiu, Q. S., & Fratti, R. A. (2010). The Na+/H+ exchanger Nhx1p regulates the initiation of
499 Saccharomyces cerevisiae vacuole fusion. *Journal of cell science*, *123*(Pt 19), 3266–3275.
500 doi:10.1242/jcs.067637. https://doi.org/10.1242/jcs.067637
501 14. Zieger, M., & Mayer, A. (2012). Yeast vacuoles fragment in an asymmetrical two-phase
502 process with distinct protein requirements. *Molecular biology of the cell*, *23*(17), 3438–
503 3449. doi:10.1091/mbc.E12-05-0347. https://doi.org/10.1091/mbc.E12-05-0347
504 15. Peters, C., Baars, T. L., Bühler, S., & Mayer, A. (2004). Mutual control of membrane
505 fission and fusion proteins. *Cell*, *119*(5), 667–678. doi:10.1016/j.cell.2004.11.023.
506 https://doi.org/10.1016/j.cell.2004.11.023
507 16. Weisman L. S. (2006). Organelles on the move: insights from yeast vacuole
508 inheritance. *Nature reviews. Molecular cell biology*, *7*(4), 243–252.
509 doi:10.1038/nrm1892. https://doi.org/10.1038/nrm1892
510 17. Efe, J. A., Botelho, R. J., & Emr, S. D. (2005). The Fab1 phosphatidylinositol kinase
511 pathway in the regulation of vacuole morphology. *Current opinion in cell biology*, *17*(4),
512 402–408. doi:10.1016/j.ceb.2005.06.002. https://doi.org/10.1016/j.ceb.2005.06.002

513 18. Efe, J. A., Botelho, R. J., & Emr, S. D. (2007). Atg18 regulates organelle morphology and
514 Fab1 kinase activity independent of its membrane recruitment by phosphatidylinositol
515 3,5-bisphosphate. *Molecular biology of the cell*, *18*(11), 4232–4244.
516 doi:10.1091/mbc.e07-04-0301. https://doi.org/10.1091/mbc.e07-04-0301
517 19. Michaillat, L., Baars, T. L., & Mayer, A. (2012). Cell-free reconstitution of vacuole
518 membrane fragmentation reveals regulation of vacuole size and number by
519 TORC1. *Molecular biology of the cell*, *23*(5), 881–895. doi:10.1091/mbc.E11-08-0703.
520 https://doi.org/10.1091/mbc.E11-08-0703
521 20. Stauffer, B., & Powers, T. (2015). Target of rapamycin signaling mediates vacuolar fission
522 caused by endoplasmic reticulum stress in Saccharomyces cerevisiae. *Molecular biology*
523 *of the cell*, *26*(25), 4618–4630. doi:10.1091/mbc.E15-06-0344.
524 https://doi.org/10.1091/mbc.E15-06-0344
525 21. Manandhar, S. P., Siddiqah, I. M., Cocca, S. M., & Gharakhanian, E. (2020). A kinase
526 cascade on the yeast lysosomal vacuole regulates its membrane dynamics: conserved
527 kinase Env7 is phosphorylated by casein kinase Yck3. *The Journal of biological*
528 *chemistry*, *295*(34), 12262–12278. doi:10.1074/jbc.RA119.012346.
529 https://doi.org/10.1074/jbc.RA119.012346
530 22. Wu, H., Carvalho, P., & Voeltz, G. K. (2018). Here, there, and everywhere: The
531 importance of ER membrane contact sites. *Science (New York, N.Y.)*, *361*(6401),
532 eaan5835. doi:10.1126/science.aan5835. https://doi.org/10.1126/science.aan5835
533 23. Prinz, W. A., Toulmay, A., & Balla, T. (2020). The functional universe of membrane
534 contact sites. *Nature reviews. Molecular cell biology*, *21*(1), 7–24. doi:10.1038/s41580-
535 019-0180-9. https://doi.org/10.1038/s41580-019-0180-9
536 24. Wickner, W., & Rizo, J. (2017). A cascade of multiple proteins and lipids catalyzes
537 membrane fusion. *Molecular biology of the cell*, *28*(6), 707–711. doi:10.1091/mbc.E16-
538 07-0517. https://doi.org/10.1091/mbc.E16-07-0517
539 25. Starr, M. L., & Fratti, R. A. (2019). The Participation of Regulatory Lipids in Vacuole
540 Homotypic Fusion. *Trends in biochemical sciences*, *44*(6), 546–554.
541 doi:10.1016/j.tibs.2018.12.003. https://doi.org/10.1016/j.tibs.2018.12.003

542 26. Ungermann, C., & Kümmel, D. (2019). Structure of membrane tethers and their role in
543 fusion. *Traffic (Copenhagen, Denmark)*, *20*(7), 479–490. doi:10.1111/tra.12655.
544 https://doi.org/10.1111/tra.12655
545 27. Hurst, L. R., & Fratti, R. A. (2020). Lipid Rafts, Sphingolipids, and Ergosterol in Yeast
546 Vacuole Fusion and Maturation. *Frontiers in cell and developmental biology*, *8*, 539.
547 doi:10.3389/fcell.2020.00539. https://doi.org/10.3389/fcell.2020.00539
548 28. Pan, X., Roberts, P., Chen, Y., Kvam, E., Shulga, N., Huang, K., Lemmon, S., & Goldfarb, D.
549 S. (2000). Nucleus-vacuole junctions in Saccharomyces cerevisiae are formed through
550 the direct interaction of Vac8p with Nvj1p. *Molecular biology of the cell*, *11*(7), 2445–
551 2457. doi:10.1091/mbc.11.7.2445. https://doi.org/10.1091/mbc.11.7.2445
552 29. Elbaz-Alon, Y., Rosenfeld-Gur, E., Shinder, V., Futerman, A. H., Geiger, T., & Schuldiner,
553 M. (2014). A dynamic interface between vacuoles and mitochondria in
554 yeast. *Developmental cell*, *30*(1), 95–102. doi:10.1016/j.devcel.2014.06.007.
555 https://doi.org/10.1016/j.devcel.2014.06.007
556 30. Hönscher, C., Mari, M., Auffarth, K., Bohnert, M., Griffith, J., Geerts, W., van der Laan,
557 M., Cabrera, M., Reggiori, F., & Ungermann, C. (2014). Cellular metabolism regulates
558 contact sites between vacuoles and mitochondria. *Developmental cell*, *30*(1), 86–94.
559 doi:10.1016/j.devcel.2014.06.006. https://doi.org/10.1016/j.devcel.2014.06.006
560 31. González Montoro, A., Auffarth, K., Hönscher, C., Bohnert, M., Becker, T., Warscheid, B.,
561 Reggiori, F., van der Laan, M., Fröhlich, F., & Ungermann, C. (2018). Vps39 Interacts with
562 Tom40 to Establish One of Two Functionally Distinct Vacuole-Mitochondria Contact
563 Sites. *Developmental cell*, *45*(5), 621–636.e7. doi:10.1016/j.devcel.2018.05.011.
564 https://doi.org/10.1016/j.devcel.2018.05.011
565 32. Murley, A., Sarsam, R. D., Toulmay, A., Yamada, J., Prinz, W. A., & Nunnari, J. (2015). Ltc1
566 is an ER-localized sterol transporter and a component of ER-mitochondria and ER-
567 vacuole contacts. *The Journal of cell biology*, *209*(4), 539–548.
568 doi:10.1083/jcb.201502033. https://doi.org/10.1083/jcb.201502033
569 33. Murley, A., Yamada, J., Niles, B. J., Toulmay, A., Prinz, W. A., Powers, T., & Nunnari, J.
570 (2017). Sterol transporters at membrane contact sites regulate TORC1 and TORC2
571 signaling. *The Journal of cell biology*, *216*(9), 2679–2689.

572 34. Reinisch, K. M., & Prinz, W. A. (2021). Mechanisms of nonvesicular lipid transport. *The*
573 *Journal of cell biology*, *220*(3), e202012058. doi:10.1083/jcb.201610032.
574 https://doi.org/10.1083/jcb.201610032
575 35. Girik, V., Feng, S., Hariri, H., Henne, W. M., & Riezman, H. (2022). Vacuole-Specific Lipid
576 Release for Tracking Intracellular Lipid Metabolism and Transport in Saccharomyces
577 cerevisiae. *ACS chemical biology*, 17(6), 1485–1494. doi:10.1021/acschembio.2c00120.
578 https://doi.org/10.1021/acschembio.2c00120
579 36. Manford, A. G., Stefan, C. J., Yuan, H. L., Macgurn, J. A., & Emr, S. D. (2012). ER-to-
580 plasma membrane tethering proteins regulate cell signaling and ER
581 morphology. *Developmental cell*, *23*(6), 1129–1140. doi:10.1016/j.devcel.2012.11.004.
582 https://doi.org/10.1016/j.devcel.2012.11.004
583 37. Ikeda, A., Schlarmann, P., Kurokawa, K., Nakano, A., Riezman, H., & Funato, K. (2020).
584 Tricalbins Are Required for Non-vesicular Ceramide Transport at ER-Golgi Contacts and
585 Modulate Lipid Droplet Biogenesis. *iScience*, *23*(10), 101603.
586 doi:10.1016/j.isci.2020.101603. https://doi.org/10.1016/j.isci.2020.101603
587 38. Toulmay, A., & Prinz, W. A. (2012). A conserved membrane-binding domain targets
588 proteins to organelle contact sites. *Journal of cell science*, *125*(Pt 1), 49–58.
589 doi:10.1242/jcs.085118. https://doi.org/10.1242/jcs.085118
590 39. Quon, E., Sere, Y. Y., Chauhan, N., Johansen, J., Sullivan, D. P., Dittman, J. S., Rice, W. J.,
591 Chan, R. B., Di Paolo, G., Beh, C. T., & Menon, A. K. (2018). Endoplasmic reticulum-
592 plasma membrane contact sites integrate sterol and phospholipid regulation. *PLoS*
593 *biology*, *16*(5), e2003864. doi:10.1371/journal.pbio.2003864.
594 https://doi.org/10.1371/journal.pbio.2003864
595 40. Jorgensen, J. R., Tei, R., Baskin, J. M., Michel, A. H., Kornmann, B., & Emr, S. D. (2020).
596 ESCRT-III and ER-PM contacts maintain lipid homeostasis. *Molecular biology of the cell*,
597 *31*(12), 1302–1313. doi:10.1091/mbc.E20-01-0061. https://doi.org/10.1091/mbc.E20-
598 01-0061
599 41. Hoffmann, P. C., Bharat, T., Wozny, M. R., Boulanger, J., Miller, E. A., & Kukulski, W.
600 (2019). Tricalbins Contribute to Cellular Lipid Flux and Form Curved ER-PM Contacts that
601 Are Bridged by Rod-Shaped Structures. *Developmental cell*, *51*(4), 488–502.e8.
602 doi:10.1016/j.devcel.2019.09.019. https://doi.org/10.1016/j.devcel.2019.09.019

603 42. Collado, J., Kalemanov, M., Campelo, F., Bourgoint, C., Thomas, F., Loewith, R.,
604 Martínez-Sánchez, A., Baumeister, W., Stefan, C. J., & Fernández-Busnadiego, R. (2019).
605 Tricalbin-Mediated Contact Sites Control ER Curvature to Maintain Plasma Membrane
606 Integrity. *Developmental cell*, 51(4), 476–487.e7. doi:10.1016/j.devcel.2019.10.018.
607 https://doi.org/10.1016/j.devcel.2019.10.018
608 43. Nelson, H., & Nelson, N. (1990). Disruption of genes encoding subunits of yeast vacuolar
609 H(+)-ATPase causes conditional lethality. *Proceedings of the National Academy of*
610 *Sciences of the United States of America*, *87*(9), 3503–3507.
611 doi:10.1073/pnas.87.9.3503. https://doi.org/10.1073/pnas.87.9.3503
612 44. Coonrod, E. M., Graham, L. A., Carpp, L. N., Carr, T. M., Stirrat, L., Bowers, K., Bryant, N.
613 J., & Stevens, T. H. (2013). Homotypic vacuole fusion in yeast requires organelle
614 acidification and not the V-ATPase membrane domain. *Developmental cell*, *27*(4), 462–
615 468. doi:10.1016/j.devcel.2013.10.014. https://doi.org/10.1016/j.devcel.2013.10.014
616 45. Seeley, E. S., Kato, M., Margolis, N., Wickner, W., & Eitzen, G. (2002). Genomic analysis
617 of homotypic vacuole fusion. *Molecular biology of the cell*, *13*(3), 782–794.
618 doi:10.1091/mbc.01-10-0512. https://doi.org/10.1091/mbc.01-10-0512
619 46. Katzmann, D. J., Babst, M., & Emr, S. D. (2001). Ubiquitin-dependent sorting into the
620 multivesicular body pathway requires the function of a conserved endosomal protein
621 sorting complex, ESCRT-I. *Cell*, 106(2), 145–155. doi:10.1016/s0092-8674(01)00434-2.
622 https://doi.org/10.1016/s0092-8674(01)00434-2
623 47. Babst, M., Sato, T. K., Banta, L. M., & Emr, S. D. (1997). Endosomal transport function in
624 yeast requires a novel AAA-type ATPase, Vps4p. *The EMBO journal*, 16(8), 1820–1831.
625 doi:10.1093/emboj/16.8.1820. https://doi.org/10.1093/emboj/16.8.1820
626 48. Stuchell-Brereton, M. D., Skalicky, J. J., Kieffer, C., Karren, M. A., Ghaffarian, S., &
627 Sundquist, W. I. (2007). ESCRT-III recognition by VPS4 ATPases. *Nature*, 449(7163), 740–
628 744. doi:10.1038/nature06172. https://doi.org/10.1038/nature06172
629 49. Dove, S. K., Dong, K., Kobayashi, T., Williams, F. K., & Michell, R. H. (2009).
630 Phosphatidylinositol 3,5-bisphosphate and Fab1p/PIKfyve underPPIn endo-lysosome
631 function. *The Biochemical journal*, *419*(1), 1–13. doi:10.1042/BJ20081950.
632 https://doi.org/10.1042/BJ20081950

633 50. Creutz, C. E., Snyder, S. L., & Schulz, T. A. (2004). Characterization of the yeast tricalbins:
634 membrane-bound multi-C2-domain proteins that form complexes involved in
635 membrane trafficking. *Cellular and molecular life sciences : CMLS*, 61(10), 1208–1220.
636 doi:10.1007/s00018-004-4029-8. https://doi.org/10.1007/s00018-004-4029-8
637 51. Tarassov, K., Messier, V., Landry, C. R., Radinovic, S., Serna Molina, M. M., Shames, I.,
638 Malitskaya, Y., Vogel, J., Bussey, H., & Michnick, S. W. (2008). An in vivo map of the
639 yeast protein interactome. *Science (New York, N.Y.)*, 320(5882), 1465–1470.
640 doi:10.1126/science.1153878. https://doi.org/10.1126/science.1153878
641 52. Michaelis, A. C., Brunner, A. D., Zwiebel, M., Meier, F., Strauss, M. T., Bludau, I., & Mann,
642 M. (2023). The social and structural architecture of the yeast protein interactome.
643 *Nature*, 624(7990), 192–200. doi:10.1038/s41586-023-06739-5.
644 https://doi.org/10.1038/s41586-023-06739-5
645 53. Omnus, D. J., Manford, A. G., Bader, J. M., Emr, S. D., & Stefan, C. J. (2016).
646 Phosphoinositide kinase signaling controls ER-PM cross-talk. *Molecular biology of the*
647 *cell*, *27*(7), 1170–1180. doi:10.1091/mbc.E16-01-0002.
648 https://doi.org/10.1091/mbc.E16-01-0002
649 54. Megyeri, M., Prasad, R., Volpert, G., Sliwa-Gonzalez, A., Haribowo, A. G., Aguilera-
650 Romero, A., Riezman, H., Barral, Y., Futerman, A. H., & Schuldiner, M. (2019). Yeast
651 ceramide synthases, Lag1 and Lac1, have distinct substrate specificity. *Journal of cell*
652 *science*, *132*(12), jcs228411. doi:10.1242/jcs.228411.
653 https://doi.org/10.1242/jcs.228411
654 55. Funato, K., Lombardi, R., Vallee, B., & Riezman, H. (2003). Lcb4p is a key regulator of
655 ceramide synthesis from exogenous long chain sphingoid base in Saccharomyces
656 cerevisiae. *The Journal of biological chemistry*, *278*(9), 7325–7334.
657 doi:10.1074/jbc.M209925200. https://doi.org/10.1074/jbc.M209925200
658 56. Qie, L., Nagiec, M. M., Baltisberger, J. A., Lester, R. L., & Dickson, R. C. (1997).
659 Identification of a Saccharomyces gene, LCB3, necessary for incorporation of exogenous
660 long chain bases into sphingolipids. *The Journal of biological chemistry*, *272*(26), 16110–
661 16117. doi:10.1074/jbc.272.26.16110. https://doi.org/10.1074/jbc.272.26.16110
662 57. Nagiec, M. M., Skrzypek, M., Nagiec, E. E., Lester, R. L., & Dickson, R. C. (1998). The LCB4
663 (YOR171c) and LCB5 (YLR260w) genes of Saccharomyces encode sphingoid long chain

664 base kinases. *The Journal of biological chemistry*, *273*(31), 19437–19442.
665 doi:10.1074/jbc.273.31.19437. https://doi.org/10.1074/jbc.273.31.19437
666 58. Mao, C., Saba, J. D., & Obeid, L. M. (1999). The dihydrosphingosine-1-phosphate
667 phosphatases of Saccharomyces cerevisiae are important regulators of cell proliferation
668 and heat stress responses. *The Biochemical journal*, 342 Pt 3(Pt 3), 667–675. PMID:
669 10477278; PMCID: PMC1220508.
670 59. Hait, N. C., Fujita, K., Lester, R. L., & Dickson, R. C. (2002). Lcb4p sphingoid base kinase
671 localizes to the Golgi and late endosomes. *FEBS letters*, 532(1-2), 97–102.
672 doi:10.1016/s0014-5793(02)03636-0. https://doi.org/10.1016/s0014-5793(02)03636-0
673 60. Iwaki, S., Sano, T., Takagi, T., Osumi, M., Kihara, A., & Igarashi, Y. (2007). Intracellular
674 trafficking pathway of yeast long-chain base kinase Lcb4, from its synthesis to its
675 degradation. *The Journal of biological chemistry*, 282(39), 28485–28492.
676 doi:10.1074/jbc.M701607200. https://doi.org/10.1074/jbc.M701607200
677 61. Kihara, A., & Igarashi, Y. (2002). Identification and characterization of a Saccharomyces
678 cerevisiae gene, RSB1, involved in sphingoid long-chain base release. *The Journal of*
679 *biological chemistry*, *277*(33), 30048–30054. doi:10.1074/jbc.M203385200.
680 https://doi.org/10.1074/jbc.M203385200
681 62. Funato, K., & Riezman, H. (2001). Vesicular and nonvesicular transport of ceramide from
682 ER to the Golgi apparatus in yeast. *The Journal of cell biology*, 155(6), 949–959.
683 doi:10.1083/jcb.200105033. https://doi.org/10.1083/jcb.200105033
684 63. Henne, W. M., Zhu, L., Balogi, Z., Stefan, C., Pleiss, J. A., & Emr, S. D. (2015).
685 Mdm1/Snx13 is a novel ER-endolysosomal interorganelle tethering protein. *The Journal*
686 *of cell biology*, 210(4), 541–551. doi:10.1083/jcb.201503088.
687 https://doi.org/10.1083/jcb.201503088
688 64. Manzanares-Estreder, S., Pascual-Ahuir, A., & Proft, M. (2017). Stress-Activated
689 Degradation of Sphingolipids Regulates Mitochondrial Function and Cell Death in Yeast.
690 *Oxidative medicine and cellular longevity*, *2017*, 2708345. doi:10.1155/2017/2708345.
691 https://doi.org/10.1155/2017/2708345
692 65. Haak, D., Gable, K., Beeler, T., & Dunn, T. (1997). Hydroxylation of Saccharomyces
693 cerevisiae ceramides requires Sur2p and Scs7p. *The Journal of biological chemistry*,

694 272(47), 29704–29710. doi:10.1074/jbc.272.47.29704.
695 https://doi.org/10.1074/jbc.272.47.29704
696 66. Brice, S. E., Alford, C. W., & Cowart, L. A. (2009). Modulation of sphingolipid metabolism
697 by the phosphatidylinositol-4-phosphate phosphatase Sac1p through regulation of
698 phosphatidylinositol in Saccharomyces cerevisiae. *The Journal of biological*
699 *chemistry*, *284*(12), 7588–7596. doi:10.1074/jbc.M808325200.
700 https://doi.org/10.1074/jbc.M808325200
701 67. Fröhlich, F., Petit, C., Kory, N., Christiano, R., Hannibal-Bach, H. K., Graham, M., Liu, X.,
702 Ejsing, C. S., Farese, R. V., & Walther, T. C. (2015). The GARP complex is required for
703 cellular sphingolipid homeostasis. *eLife*, 4, e08712. doi:
704 10.7554/eLife.08712. https://doi.org/10.7554/eLife.08712
705 68. Hepowit, N. L., Moon, B., Ebert, A. C., Dickson, R. C., & MacGurn, J. A. (2023). Art2
706 mediates selective endocytosis of methionine transporters during adaptation to
707 sphingolipid depletion. *Journal of cell science*, 136(14), jcs260675. doi:
708 10.1242/jcs.260675. https://doi.org/10.1242/jcs.260675
709 69. Malia, P. C., Numrich, J., Nishimura, T., González Montoro, A., Stefan, C. J., &
710 Ungermann, C. (2018). Control of vacuole membrane homeostasis by a resident PI-3,5-
711 kinase inhibitor. *Proceedings of the National Academy of Sciences of the United States of*
712 *America*, *115*(18), 4684–4689. doi:10.1073/pnas.1722517115.
713 https://doi.org/10.1073/pnas.1722517115
714 70. Chen, Z., Malia, P. C., Hatakeyama, R., Nicastro, R., Hu, Z., Péli-Gulli, M. P., Gao, J.,
715 Nishimura, T., Eskes, E., Stefan, C. J., Winderickx, J., Dengjel, J., De Virgilio, C., &
716 Ungermann, C. (2021). TORC1 Determines Fab1 Lipid Kinase Function at Signaling
717 Endosomes and Vacuoles. *Current biology : CB*, *31*(2), 297–309.e8.
718 doi:10.1016/j.cub.2020.10.026. https://doi.org/10.1016/j.cub.2020.10.026
719 71. Gopaldass, N., Fauvet, B., Lashuel, H., Roux, A., & Mayer, A. (2017). Membrane scission
720 driven by the PROPPIN Atg18. *The EMBO journal*, *36*(22), 3274–3291.
721 doi:10.15252/embj.201796859. https://doi.org/10.15252/embj.201796859
722 72. Jin, N., Mao, K., Jin, Y., Tevzadze, G., Kauffman, E. J., Park, S., Bridges, D., Loewith, R.,
723 Saltiel, A. R., Klionsky, D. J., & Weisman, L. S. (2014). Roles for PI(3,5)P2 in nutrient

724 sensing through TORC1. *Molecular biology of the cell*, *25*(7), 1171–1185.
725 doi:10.1091/mbc.E14-01-0021. https://doi.org/10.1091/mbc.E14-01-0021
726 73. Hannun, Y. A., Loomis, C. R., Merrill, A. H., Jr, & Bell, R. M. (1986). Sphingosine inhibition
727 of protein kinase C activity and of phorbol dibutyrate binding in vitro and in human
728 platelets. *The Journal of biological chemistry*, *261*(27), 12604–12609. PMID: 3462188.
729 74. Chang, H. C., Tsai, L. H., Chuang, L. Y., & Hung, W. C. (2001). Role of AKT kinase in
730 sphingosine-induced apoptosis in human hepatoma cells. *Journal of cellular*
731 *physiology*, *188*(2), 188–193. doi:10.1002/jcp.1108. https://doi.org/10.1002/jcp.1108
732 75. Yabuki, Y., Ikeda, A., Araki, M., Kajiwara, K., Mizuta, K., & Funato, K. (2019).
733 Sphingolipid/Pkh1/2-TORC1/Sch9 Signaling Regulates Ribosome Biogenesis in
734 Tunicamycin-Induced Stress Response in Yeast. *Genetics*, *212*(1), 175–186.
735 doi:10.1534/genetics.118.301874. https://doi.org/10.1534/genetics.118.301874
736 76. Zhukovsky, M. A., Filograna, A., Luini, A., Corda, D., & Valente, C. (2019). Protein
737 Amphipathic Helix Insertion: A Mechanism to Induce Membrane Fission. *Frontiers in cell*
738 *and developmental biology*, *7*, 291. doi:10.3389/fcell.2019.00291.
739 https://doi.org/10.3389/fcell.2019.00291
740 77. Contreras, F. X., Sot, J., Alonso, A., & Goñi, F. M. (2006). Sphingosine increases the
741 permeability of model and cell membranes. *Biophysical journal*, *90*(11), 4085–4092.
742 doi:10.1529/biophysj.105.076471. https://doi.org/10.1529/biophysj.105.076471
743 78. Siskind, L. J., Fluss, S., Bui, M., & Colombini, M. (2005). Sphingosine forms channels in
744 membranes that differ greatly from those formed by ceramide. *Journal of bioenergetics*
745 *and biomembranes*, *37*(4), 227–236. doi:10.1007/s10863-005-6632-2.
746 https://doi.org/10.1007/s10863-005-6632-2
747 79. Jiménez-Rojo, N., Sot, J., Viguera, A. R., Collado, M. I., Torrecillas, A., Gómez-Fernández,
748 J. C., Goñi, F. M., & Alonso, A. (2014). Membrane permeabilization induced by
749 sphingosine: effect of negatively charged lipids. *Biophysical journal*, *106*(12), 2577–
750 2584. doi:10.1016/j.bpj.2014.04.038. https://doi.org/10.1016/j.bpj.2014.04.038
751 80. Rodriguez-Gallardo, S., Kurokawa, K., Sabido-Bozo, S., Cortes-Gomez, A., Ikeda, A., Zoni,
752 V., Aguilera-Romero, A., Perez-Linero, A. M., Lopez, S., Waga, M., Araki, M., Nakano, M.,
753 Riezman, H., Funato, K., Vanni, S., Nakano, A., & Muñiz, M. (2020). Ceramide chain
754 length-dependent protein sorting into selective endoplasmic reticulum exit sites.

Science advances, 6(50), eaba8237. doi:10.1126/sciadv.aba8237. https://doi.org/10.1126/sciadv.aba8237

81. Rodriguez-Gallardo, S., Sabido-Bozo, S., Ikeda, A., Araki, M., Okazaki, K., Nakano, M., Aguilera-Romero, A., Cortes-Gomez, A., Lopez, S., Waga, M., Nakano, A., Kurokawa, K., Muñiz, M., & Funato, K. (2022). Quality-controlled ceramide-based GPI-anchored protein sorting into selective ER exit sites. *Cell reports*, 39(5), 110768. doi:10.1016/j.celrep.2022.110768. https://doi.org/10.1016/j.celrep.2022.110768
82. Ikeda, A., Hanaoka, K., & Funato, K. (2021). Protocol for measuring sphingolipid metabolism in budding yeast. *STAR protocols*, 2(2), 100412. doi:10.1016/j.xpro.2021.100412. https://doi.org/10.1016/j.xpro.2021.100412
83. Jumper, J., Evans, R., Pritzel, A., Green, T., Figurnov, M., Ronneberger, O., Tunyasuvunakool, K., Bates, R., Žídek, A., Potapenko, A., Bridgland, A., Meyer, C., Kohl, S., Ballard, A. J., Cowie, A., Romera-Paredes, B., Nikolov, S., Jain, R., Adler, J., Back, T., Petersen, S., Reiman, D., Clancy, E., Zielinski, M., Steinegger, M., Pacholska, M., Berghammer, T., Bodenstein, S., Silver, D., Vinyals, O., Senior, A. W., Kavukcuoglu, K., Kohli, P., Hassabis, D., & Hassabis, D. (2021). Highly accurate protein structure prediction with AlphaFold. *Nature*, *596*(7873), 583–589. doi:10.1038/s41586-021-03819-2. https://doi.org/10.1038/s41586-021-03819-2

Figures and legends

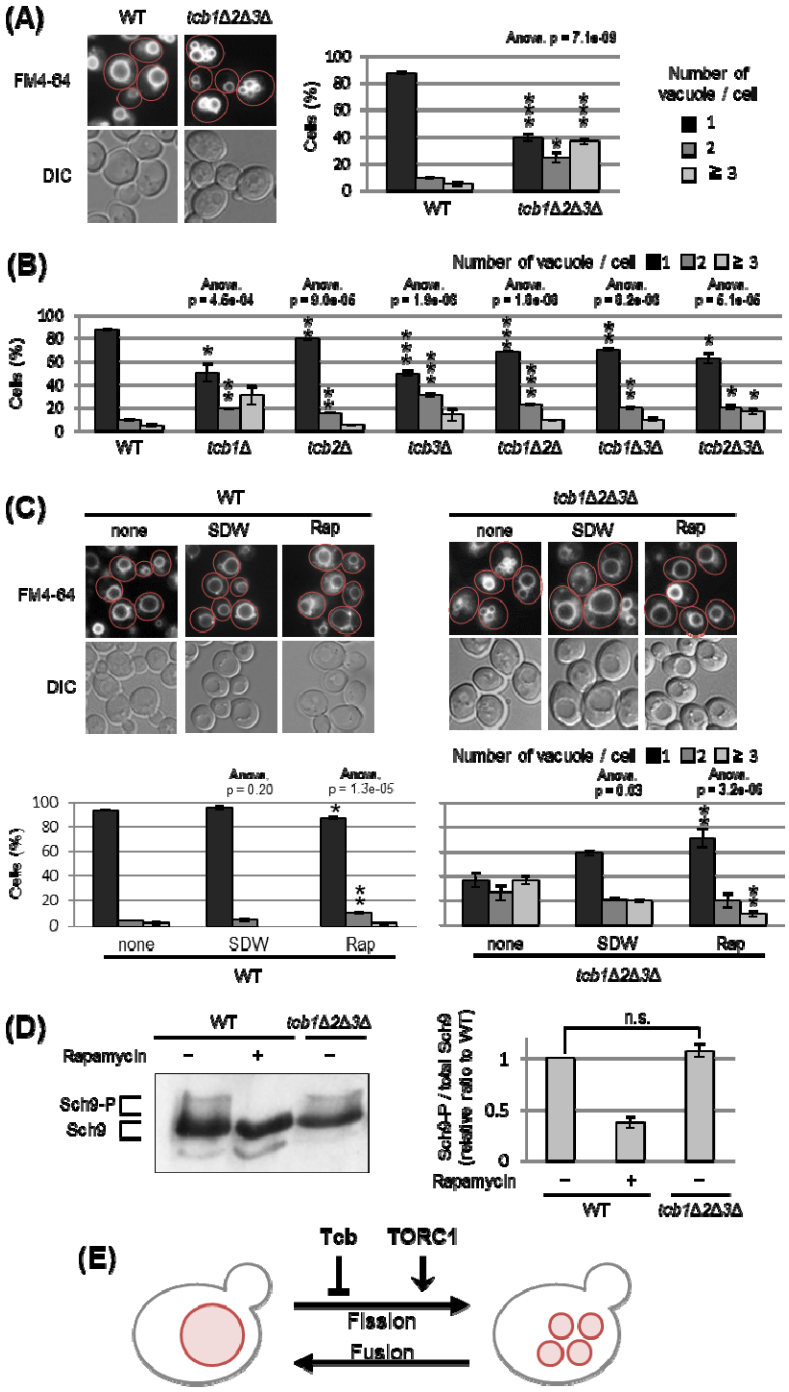

Figure 1. Deletion of tricalbin proteins causes vacuole fragmentation

(A, B) Cells (FKY2577 and FKY2927 in A; FKY2577, FKY2909, FKY3819, FKY2924, FKY3023, FKY3820 and FKY3008 in B) were grown overnight at 25 ºC in YPD. Then vacuoles were stained with FM4-64 and imaged by fluorescence microscopy. The number of vacuoles per cell was counted and categorized into one of three groups. The data represent mean ± SE of three

independent experiments, each based on more than 100 cells. *$p < 0.05$, **$p < 0.01$ and ***$p < 0.001$ by Student's t-test compared with WT.

(C) Cells (FKY2577 and FKY2927) were grown overnight at 25 ºC in YPD. Cells were then incubated in sterile distilled water (SDW) for more than 45 minutes or YPD with 200 nM of rapamycin (Rap) for 2 hours. Vacuoles were stained with FM4-64 and imaged by fluorescence microscopy. The number of vacuoles per cell was counted and categorized into one of three groups. The data represent mean ± SE of more than three independent experiments, each based on more than 100 cells. *$p < 0.05$, **$p < 0.01$ by Student's t-test compared with none treated cells.

(A-C) Significant differences analysis between the pairwise combination of groups was performed using two-way ANOVA.

(D) Cells (FKY2577 and FKY2927) transformed with pRS416-SCH9-5HA were cultured in YPD, treated with 200 nM rapamycin (control) or untreated. The extracts from cells expressing Sch9-5HA were reacted with 2-nitro-5-thiocyanobenzoic acid and analyzed by immunoblotting using anti-HA. Phosphorylated Sch9 relative to the total Sch9 was calculated and shown in comparison to untreated WT cells. The data represent mean ± SE of three independent experiments. *$p < 0.05$ by Student's t-test.

(E) Illustration shows that tricalbin proteins negatively regulate the vacuole fission in a TORC1-independent manner.

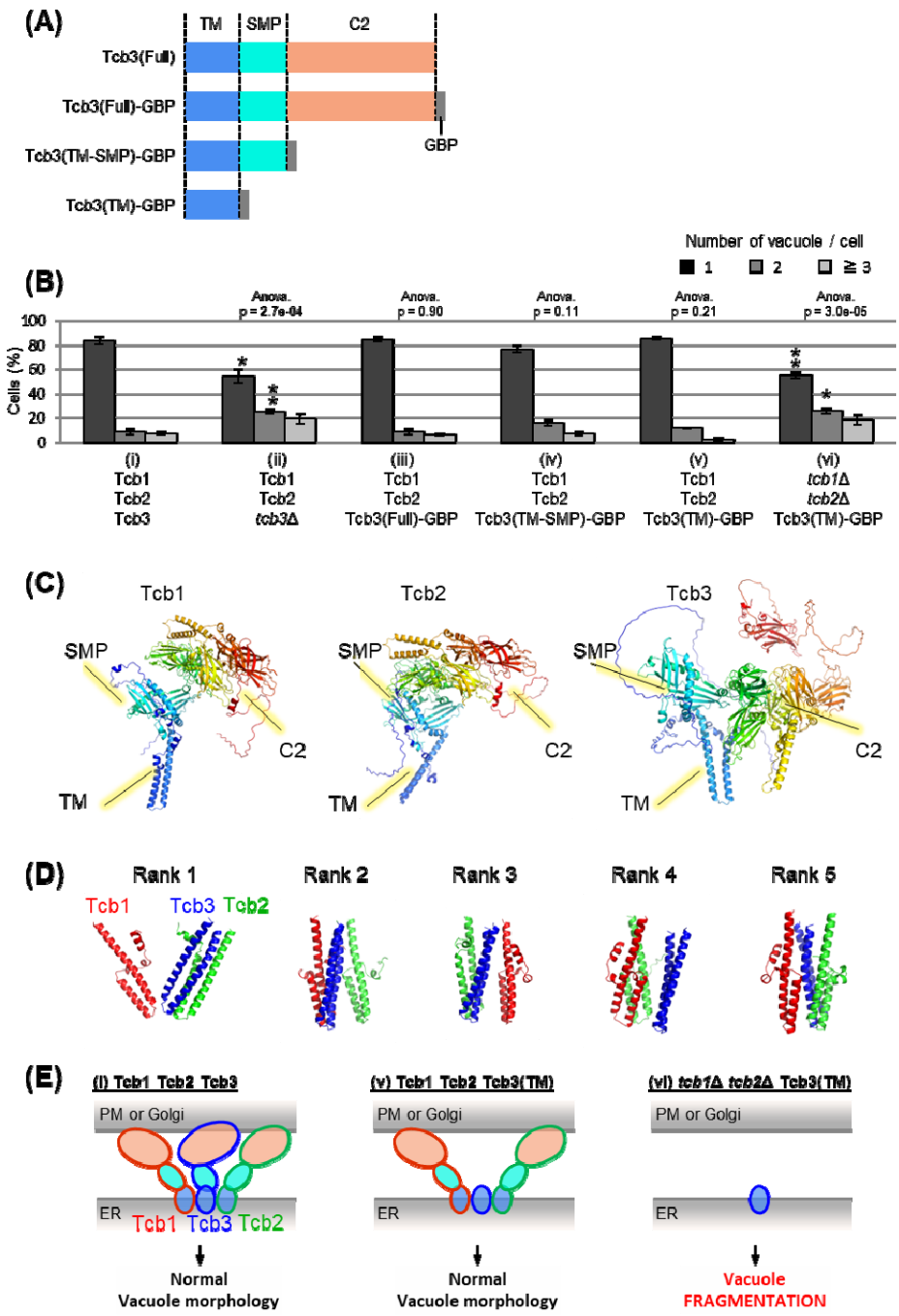

Figure 2. Effects of domain deletion and artificial tether on vacuole morphology

(A) Diagram of domain organization of Tcb3 protein. TM, transmembrane domain; SMP, synaptotagmin-like mitochondrial lipid-binding protein; C2, calcium-dependent lipid-binding domain; GBP, GFP-binding protein.

(B) Cells (FKY2577 (i), FKY2924 (ii), FKY3903 (iii), FKY3904 (iv), FKY3905 (v) and FKY4754 (vi)) were grown overnight at 25 ºC in YPD. Then vacuoles were stained with FM4-64 and imaged by

fluorescence microscopy. The number of vacuoles per cell was counted and categorized into one of three groups. The data represent mean ± SE of three independent experiments, each based on more than 100 cells. *$p < 0.05$ and **$p < 0.01$ by Student's t-test compared with Tcb1 Tcb2 Tcb3 (i). Significant differences analysis between the pairwise combination of groups was performed using two-way ANOVA.

(C) The modeled structures of the Tcb1p, Tcb2p and Tcb3p proteins. The ribbons and arrows indicate alpha-helices and beta-sheets, respectively.

(D) TM domain complex in Tcb1p (red), Tcb2p (green), and Tcb3p (blue). The rank "X" indicates the order in which the complexes are most likely to form.

(E) Illustrations show that TM domain of Tcb3 contributes to mediating protein interactions between the tricalbin family to maintain vacuolar morphology.

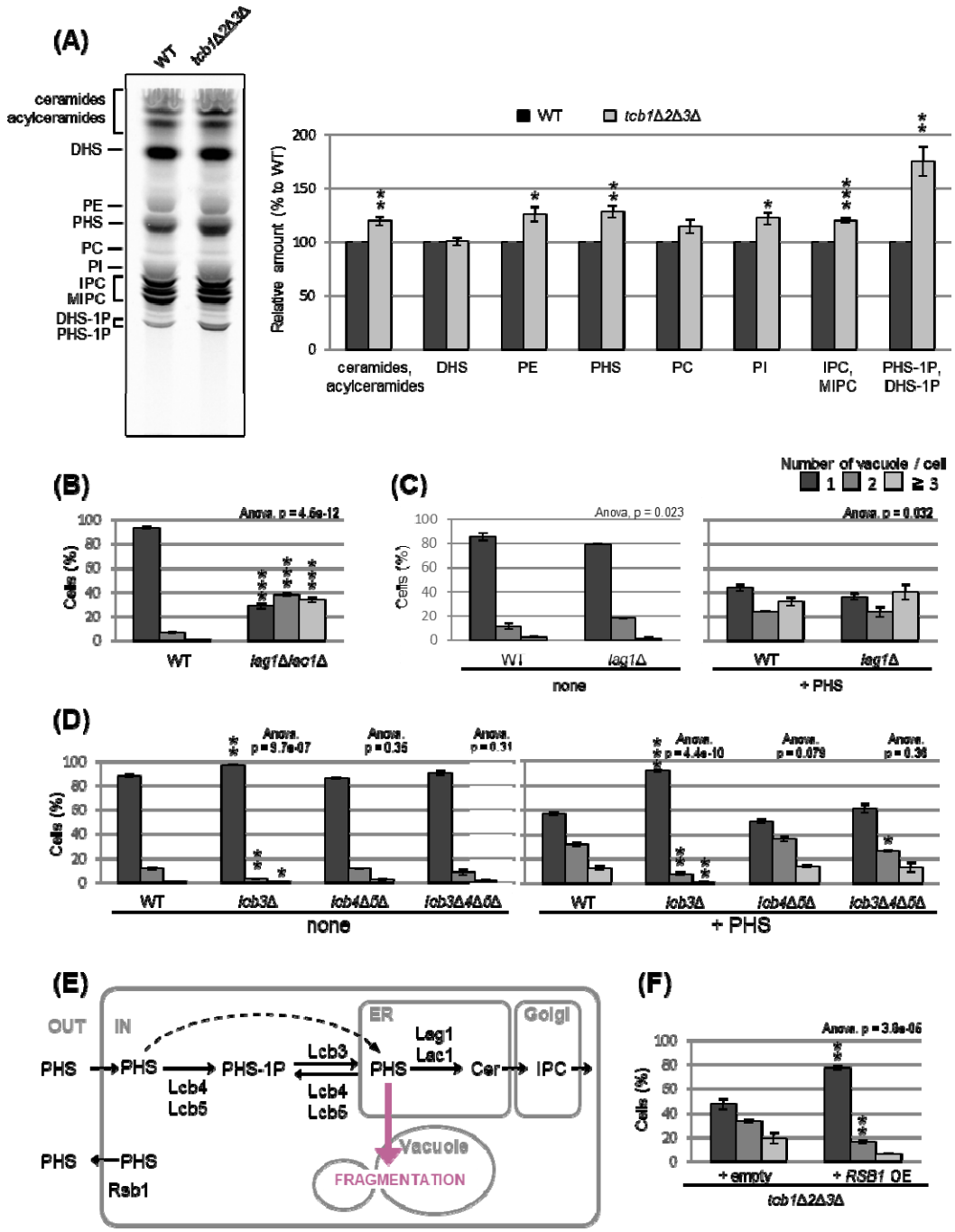

Figure 3. Accumulated PHS in *tcb1Δ2Δ3Δ* causes vacuole fragmentation.

(A) Cells (FKY2577 and FKY2927) were grown at 25˚C, and labeled with [^{3}H]DHS for 3 hours. Labelled lipids were applied to TLC plates using solvent system (Chloroform-methanol-4.2N ammonium hydroxide (9:7:2, v/v/v)). Incorporation of [^{3}H]DHS into each lipid was quantified and the percentage of the total radioactivity (%) in WT cells was determined. Data represent mean ± SE of four independent experiments. ** P < 0.01 by Student's t-test.

(B-D, F) Cells (FKY5687 and FKY5688 in B; FKY3340 and YKC121-59 in C; FKY36, FKY37, FKY33 and FKY38 in D; FKY2927 in F) were grown overnight at 25 ºC in YPD. PHS was added at 160 µM (C) or 80 µM (D) for 2 hours. Vacuoles were stained with FM4-64 and imaged by fluorescence microscopy. The number of vacuoles per cell was counted and categorized into one of three groups. The data represent mean ± SE of three independent experiments, each based on more than 100 cells. *$p < 0.05$, **$p < 0.01$ and ***$p<0.001$ by Student's t-test compared with WT (B, D) or empty cells (F). Significant differences analysis between the pairwise combination of groups was performed using two-way ANOVA.

(E) Illustration showing intracellular utilization pathway of exogenous PHS.

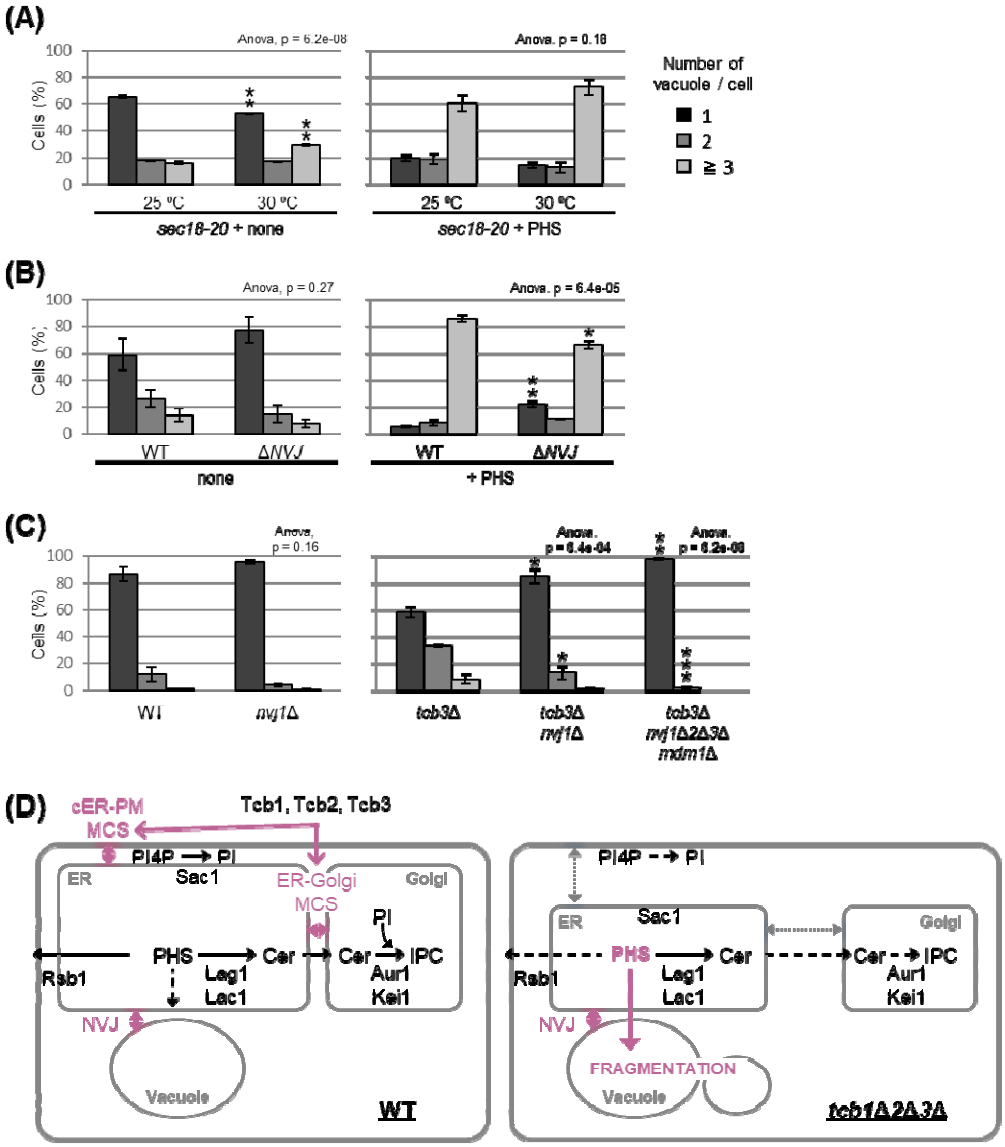

Figure 4. NVJ is required for PHS-induced vacuole fragmentation

(A-C) Cells (FKY2929 in A; FKY3868 and FKY5560 in B; FKY6187, FKY6189, FKY6190, FKY6188 and FKY6409 in C) were grown overnight at 25 ºC in YPD. PHS was added at 40 µM for 2 hours at 30 ºC (A) and 25 ºC (A, B). Vacuoles were stained with FM4-64 and imaged by fluorescence microscopy. The number of vacuoles per cell was counted and categorized into one of three groups. The data represent mean ± SE of three independent experiments, each based on more than 100 cells. *p < 0.05, **p < 0.01 and ***p<0.001 by Student's t-test. Significant differences analysis between the pairwise combination of groups was performed using two-way ANOVA.

(D) Membrane contact sites regulate vacuole morphology via sphingolipid metabolism. See the main text for details.

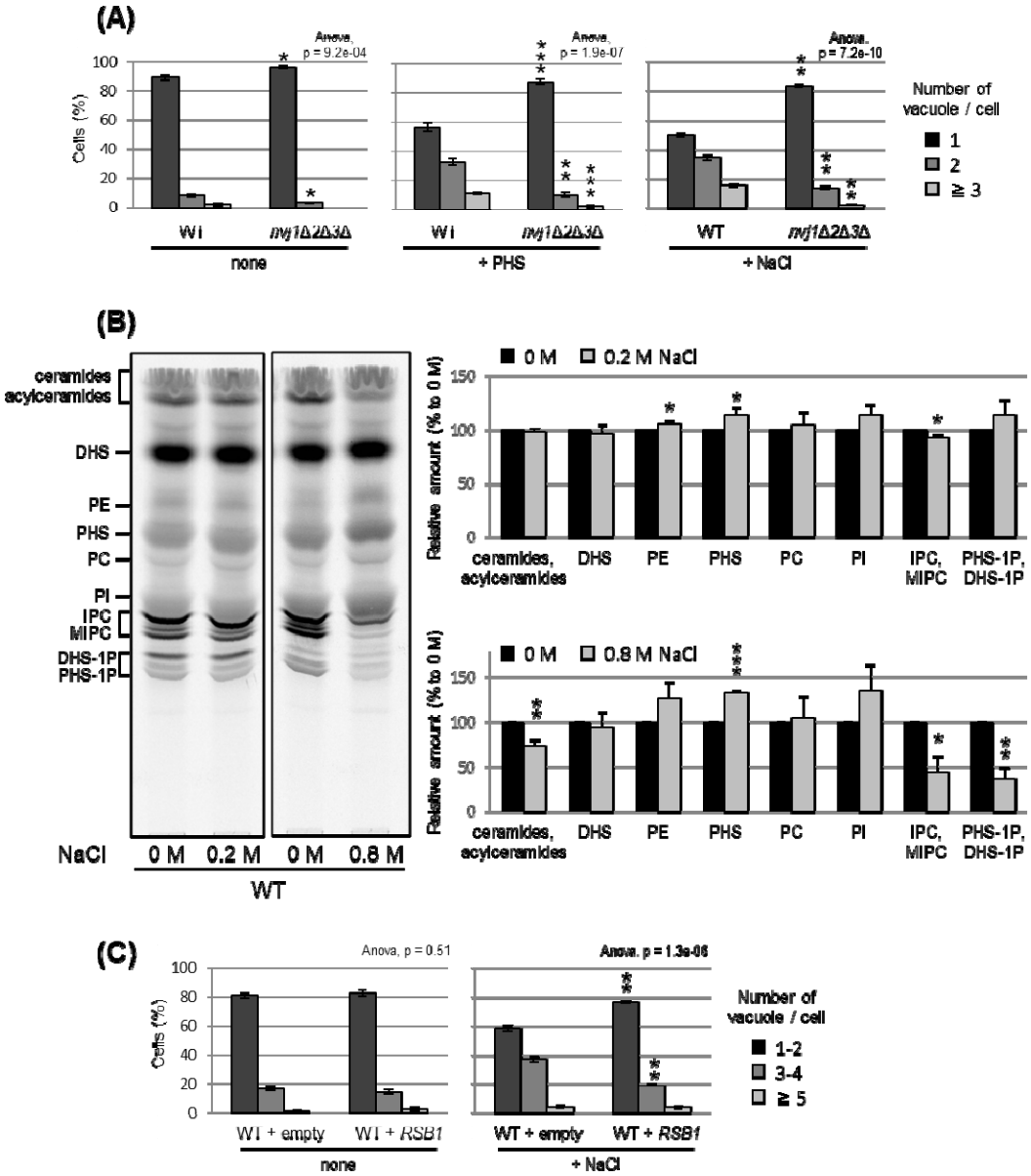

Figure 5. NVJ and PHS accumulation mediate hyperosmotic shock-induced vacuole fission

(A) Cells (FKY6187 and FKY6140) were grown overnight at 25 ºC in YPD, incubated with 80 µM of PHS or 0.2 M of NaCl for 2 hours. Vacuoles were stained with FM4-64 and imaged by fluorescence microscopy. The number of vacuoles per cell was counted and categorized into one of three groups. (B) Cells (FKY2577) were grown at 25˚C then labeled with [^{3}H]DHS and incubated with 0.2 M or 0.8 M of NaCl for 2 hours. Labelled lipids were applied to TLC plates using solvent system (Chloroform-methanol-4.2N ammonium hydroxide (9:7:2, v/v/v)).

Incorporation of [^{3}H]DHS into each lipid was quantified and the percentage of the total radioactivity (%) in WT cells was determined. Data represent mean ± SE of four independent experiments. (C) Cells (FKY2577) were grown overnight at 25 ºC in SD, then incubated with 0.2 M of NaCl for 2 hours. Vacuoles were stained with FM4-64 and imaged by fluorescence microscopy. The number of vacuoles per cell was counted and categorized into one of three groups. (A-C) The data represent mean ± SE of three independent experiments. *$p < 0.05$, **$p < 0.01$ and ***$p<0.001$ by Student's t-test. Significant differences analysis between the pairwise combination of groups was performed using two-way ANOVA.

Supplementary information

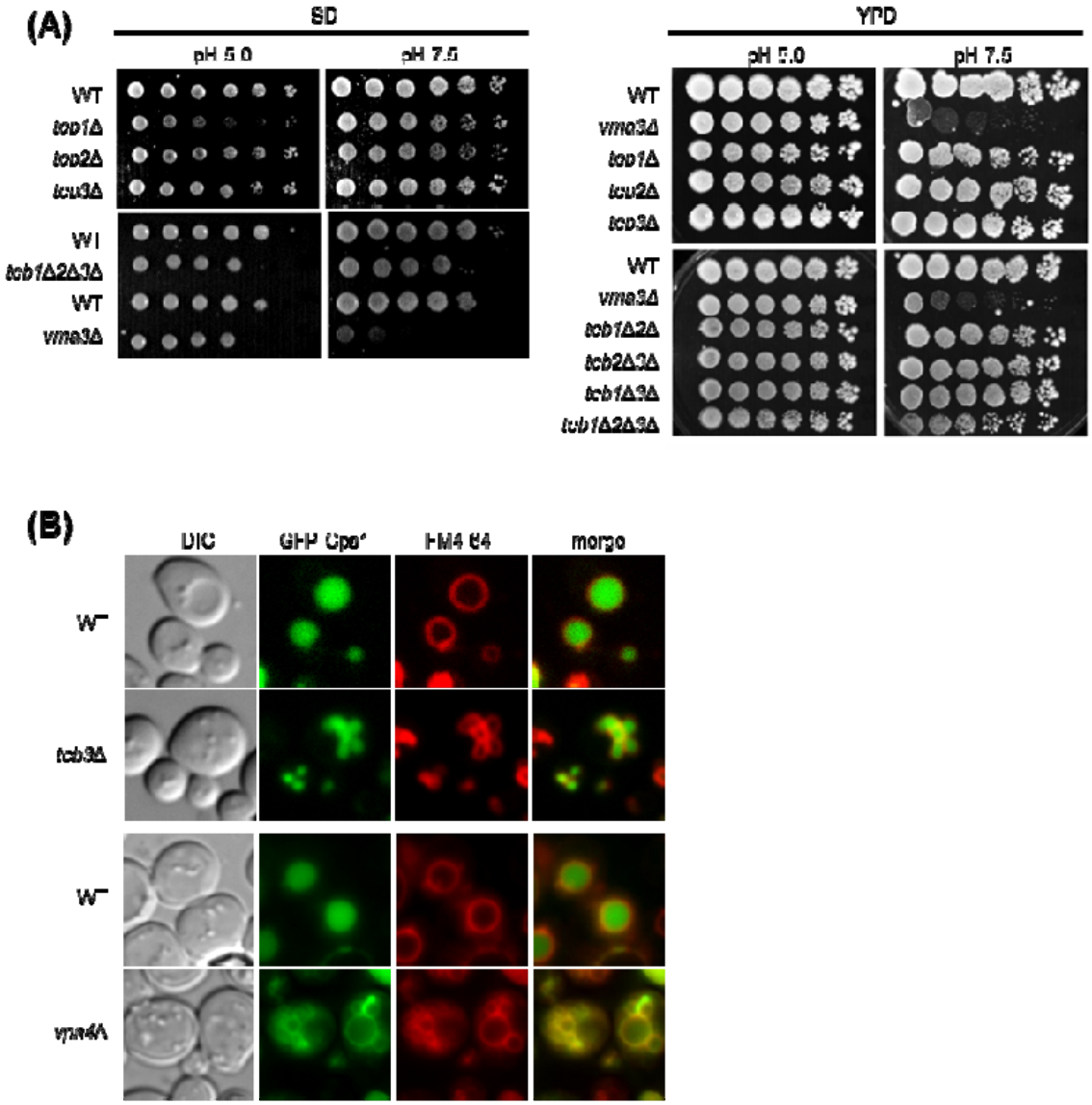

Supplementary Figure 1

(A) Cells (FKY2577, FKY2909, FKY3819, FKY2924, FKY2927, FKY3340 and YKC112-01) were adjusted to OD_{600} = 1.0 and fivefold serial dilutions were then spotted on YPD plates of indicated pH, then incubated at 25 ºC.

(B) GFP-Cps1p fusion protein was transformed into WT (FKY2577), *tcb3*Δ (FKY2924), WT (FKY3340) and *vps4*Δ (YKC149-61) strains and analyzed its subcellular localization with respect to FM4-64-stained vacuoles using by fluorescent microscopy.

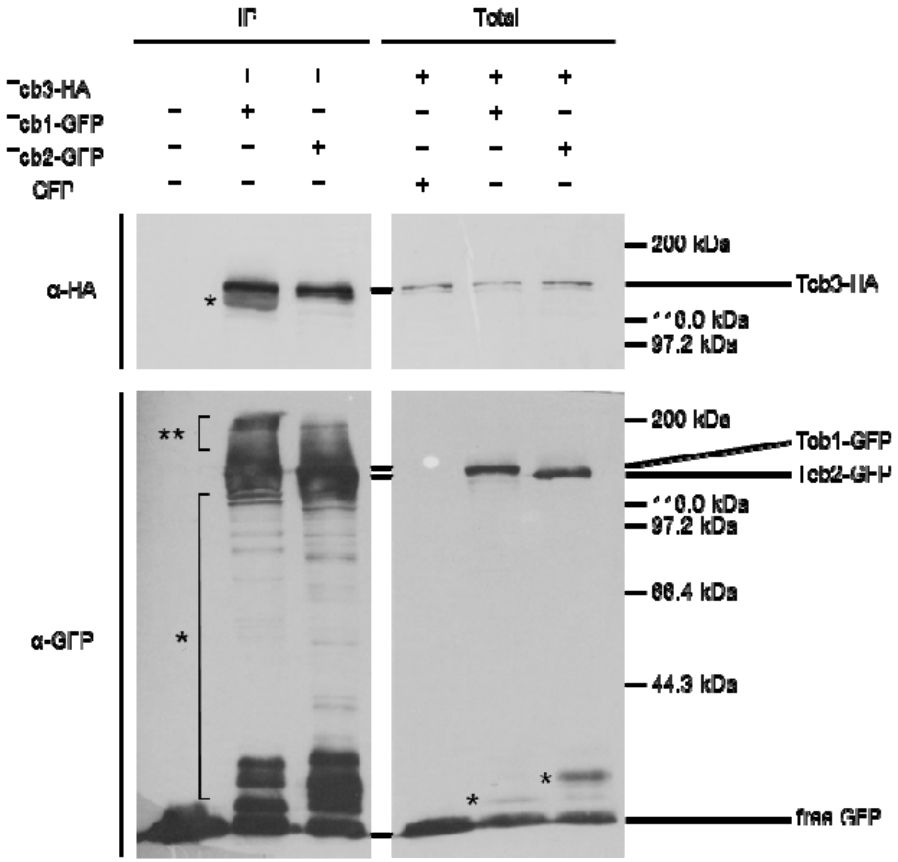

Supplementary Figure 2

Coimmunoprecipitation assay between Tcb3-HA and Tcb1-GFP or Tcb2-GFP. Tcb1-GFP (FKP1127), Tcb2-GFP (FKP1131) or GFP (FKP851) plasmids were transformed into *TCB3*-HA *pep4*Δ strain (FKY3209). Cells were grown overnight at 25 ºC in semi-SD (SD medium containing 0.2% yeast extract). Enriched ER fractions were processed for coimmunoprecipitation. Bound material (IP) was separated by SDS-PAGE and analyzed by immunoblotting using antibodies against HA and GFP. Total represents a fraction of the solubilized input material. Single star (*) indicates presumable degradation products. Double star (**) indicates presumable phosphorylation or other modification bands of Tcb1-GFP or Tcb2-GFP.

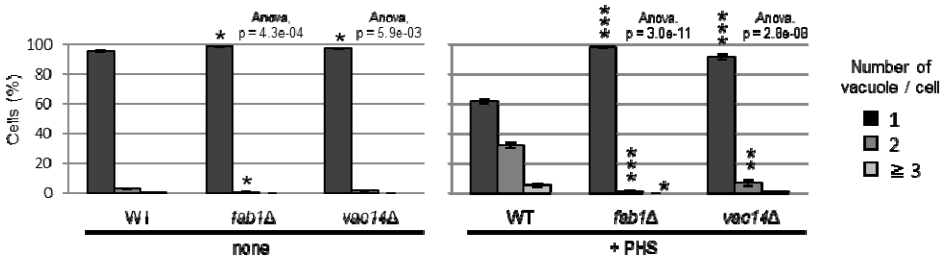

Supplementary Figure 3

Cells (FKY3340, YKC145-21 and YKC149-61) were grown overnight at 25 ºC in YPD. PHS was added at 80 µM for 2 hours. Vacuoles were stained with FM4-64 and imaged by fluorescence microscopy. The number of vacuoles per cell was counted and categorized into one of three groups. The data represent mean ± SE of three independent experiments, each based on more than 100 cells. *p < 0.05, **p < 0.01 and ***p<0.001 by Student's t-test. Significant differences analysis between the pairwise combination of groups was performed using two-way ANOVA.

Supplementary Table 1

Yeast strains used in this study, Related to All Figures.

Strain	Number	MAT	Genotype	Source
WT (RH)	FKY2577	a	*ura3 his3 leu2 trp1 lys2 bar1-1*	Ikeda A et al. iScience. 2020;23(10):101603.
tcb1 Δ*2* Δ*3* Δ	FKY2927	a	RH except for *tcb1* Δ::*TRP1 tcb2* Δ::*HIS3 tcb3* Δ::*LEU2*	Ikeda A et al. iScience. 2020;23(10):101603.
tcb1 Δ	FKY2909	a	RH except for *tcb1* Δ::*TRP1*	Ikeda A et al. iScience. 2020;23(10):101603.
tcb2 Δ	FKY3819	alpha	RH except for *tcb2* Δ::*HIS3*	Ikeda A et al. iScience. 2020;23(10):101603.
tcb3 Δ	FKY2924	a	RH except for *tcb3* Δ::*LEU2*	Ikeda A et al. iScience. 2020;23(10):101603.
tcb1 Δ*2* Δ	FKY3023	a	RH except for *tcb1* Δ::*TRP1 tcb2* Δ::*HIS3*	Ikeda A et al. iScience. 2020;23(10):101603.
tcb1 Δ*3* Δ	FKY3820	alpha	RH except for *tcb1* Δ::*TRP1 tcb3* Δ::*LEU2*	Ikeda A et al. iScience. 2020;23(10):101603.
tcb2 Δ*3* Δ	FKY3008	a	RH except for *tcb2* Δ::*HIS3 tcb3* Δ::*LEU2*	Ikeda A et al. iScience. 2020;23(10):101603.
TCB3 (Full)-GBP	FKY3903	a	RH except for *TCB3-GBP* Δ::*KanMX*	This study
TCB3 (TM-SMP)-GBP	FKY3904	a	RH except for *TCB3* (1F-489R)-*GBP* ::*KanMX*	This study
TCB3 (TM)-GBP	FKY3905	a	RH except for *TCB3* (1F-259R)-*GBP* ::*KanMX*	This study
tcb1 Δ*2* Δ *TCB3* (TM)-GBP	FKY4754	a	RH except for *tcb1* Δ::*TRP1 tcb2* Δ::*HIS3 TCB3* (1F-259R)::*KanMX*	This study
WT	FKY36 / RH4423	alpha	RH except for *HIS3* + *TRP1* + *LYS2* + *pep4-3*	Funato K et al. J Biol Chem. 2003;278(9):7325-7334.
lcb3 Δ	FKY37 / RH4427	alpha	RH except for *lcb3* Δ::KanMX *HIS3* + *LEU2* + *TRP1* + *LYS2* + *pep4-3*	Funato K et al. J Biol Chem. 2003;278(9):7325-7334.
lcb4 Δ*5* Δ	FKY33 / RH4402	alpha	RH except for *lcb4* Δ::*URA3 lcb5* Δ::*LEU2 HIS3* + *TRP1* + *LYS2* + *pep4-3*	Funato K et al. J Biol Chem. 2003;278(9):7325-7334.
lcb3 Δ*4* Δ*5* Δ	FKY38 / RH4464	alpha	RH except for *lcb3* Δ::*kanMX lcb4* Δ::*URA3 lcb5* Δ::*LEU2 HIS3* + *TRP1* + *LYS2* + *pep4-3*	Funato K et al. J Biol Chem. 2003;278(9):7325-7334.
sec18-20	FKY2929	alpha	RH except for *sec18-20 LYS2+*	Ikeda A et al. iScience. 2020;23(10):101603.
WT (RH)	FKY6187	alpha	*ura3 his3 leu2 trp1 lys2 bar1-1*	This study
nvj1 Δ	FKY6189	a	RH except for *nvj1* Δ::*HIS3*	This study
tcb3 Δ	FKY6190	alpha	RH except for *tcb3* Δ::*LEU2*	This study
tcb3 Δ*nvj1* Δ	FKY6188	a	RH except for tcb3Δ::*LEU2* nvj1Δ::HIS3	This study
tcb3 Δ*nvj1* Δ*2* Δ*3* Δ*mdm1* Δ	FKY6409	a	RH except for *nvj1* Δ:: *URA3 nvj2* Δ::*KanMX nvj3* Δ::*HIS3 mdm1* Δ::*KanMX tcb3* Δ::*LEU2*	This study
nvj1Δ2Δ3Δ	FKY6410	a	RH except for nvj1Δ:: URA3 nvj2Δ::KanMX nvj3Δ::HIS3	This study
WT (W303)	FKY5687 / RL1	a	*his3-11,15 leu2-3,112 trp1-1 ura3-1 ade2-1 can1-100 GAL + bar-*	Lucena R et al. Curr Biol. 2018;28(2):196-210.
lag1 Δ*lac1* Δ	FKY5688 / RL40	a	W303 except for *lag1* Δ::*KanMX6 lac1* Δ::*HIS*	Lucena R et al. Curr Biol. 2018;28(2):196-210.
WT (BY4742)	FKY3340	alpha	*his3* Δ*1 leu2* Δ*0 lys2* Δ*0 ura3* Δ*0*	Open biosystem, inc
lag1 Δ	YKC121-59	alpha	BY4742 except for *lag1* Δ::*KanMx*	Open biosystem, inc
vma3 Δ	YKC112-01	alpha	BY4742 except for *vma3* Δ::*KanMx*	Open biosystem, inc
vps4 Δ	YKC124-58	alpha	BY4742 except for *vps4Δ::KanMx*	Open biosystem, inc
fab1 Δ	YKC145-21	alpha	BY4742 except for *fab1* Δ::*KanMx*	Open biosystem, inc
vac14 Δ	YKC149-61	alpha	BY4742 except for *vac14* Δ::*KanMx*	Open biosystem, inc
TCB3-HA *pep4* Δ	FKY3209	alpha	BY4742 except for *TCB3-HA* ::*HIS3 pep4* Δ::*KanMx*	This study
WT (SEY6210)	FKY3868	alpha	*ura3-52 leu2-3,112 his3-Δ100 trp1-Δ901 lys2-801 suc2-Δ9*	Yabuki Y et al. Genetics. 2019;212(1):175-186.
Δ*NVJ*	FKY5560	alpha	SEY6210 except for *nvj1* Δ::*TRP1 nvj2* Δ::*HIS3 nvj3* Δ::*NatMX mdm1* Δ::*KanMX*	Henne WM et al. J Cell Biol. 2015;210(4):541-551.

Supplementary Table 2

Plasmids used in this study, Related to All Figures.

Plasmid	Number	Relevant information	Source
pRS426-*TDH3*	FKP51	2μ, yeast *TDH3* promoter, empty, *URA3*	Mumberg D et al., Gene. 1995;156(1):119-122
pRS426-*TDH3*/*RSB1*	FKP1065	2μ, yeast *TDH3* promoter, *RSB1* , *URA3*	This study
pRS316/*PTDH3*-EGFP-*CPS1*-*TCMK1*	FKP621	CEN, yeast *TDH3* promoter, GFP-*CPS1, URA3*	Provided by Riezman H
pRS416GPD/GFP	FKP851	CEN, yeast *TDH3* promoter, GFP, *URA3*	This study
pRS416GPD/*TCB1*-GFP	FKP1127	CEN, yeast *TDH3* promoter, *TCB1*-GFP, *URA3*	This study
pRS416GPD/*TCB2*-GFP	FKP1131	CEN, yeast *TDH3* promoter, *TCB2*-GFP, *URA3*	This study